

1        **LPB hydro-climate variability as simulated by GCM**  
2        **experiments: Role of remote SST forcing**

3        Annalisa Cherchi<sup>1</sup>, Andrea F Carril<sup>2,3,4</sup>, Laura Zamboni<sup>5</sup>, and Claudio Menéndez<sup>2,3,4</sup>

4        <sup>1</sup>Centro Euromediterraneo per i Cambiamenti Climatici, and Istituto Nazionale di  
5        Geofisica e Vulcanologia, Bologna, Italy

6        <sup>2</sup>Centro de Investigaciones del Mar y de la Atmósfera (CIMA), CONICET-UBA, Buenos  
7        Aires, Argentina

8        <sup>3</sup>Departamento de Ciencias de la Atmosfera y los Océanos (DCAO), FCEN, Universidad  
9        de Buenos Aires, Argentina

10        <sup>4</sup>UMI IFAECI/CNRS, Buenos Aires, Argentina

11        <sup>5</sup>Mathematics and Computer Science Division, Argonne National Laboratory, Argonne,  
12        IL, USA

13        Manuscript submitted to

14        **Climate Dynamics**

15        July 20, 2012

16        **Corresponding author:**

17        Annalisa Cherchi (CMCC/INGV)

18        Viale Aldo Moro 44

19        40127 Bologna, Italy

20        E-mail: annalisa.cherchi@bo.ingv.it

21        Phone: +39 051 3782613

22        Fax: +39 051 3782655

## Abstract

A set of AMIP-type experiments is computed and analyzed to study springtime hydro-climate variability in the region of La Plata Basin (LPB). In particular, an ensemble of nine experiments with same interannually varying SST, as boundary forcing, and different initial conditions is used to investigate the relative role of the Pacific, Indian and Atlantic tropical oceans on modulating the local precipitation. The AMIP-type ensemble results have been compared with a coupled model experiment (using the same atmospheric component). The comparison reveals that the model has a good performance in the simulation of precipitation over LPB and South America, with a slight overestimation of the seasonal mean and an underestimation of the variability. Nevertheless, an EOF analysis of South America precipitation shows that the model is able to realistically reproduce the dominant modes of variability in spring. Further, its principal component (PC1) when correlated with global SST and atmospheric fields identifies the pattern related to ENSO and the large-scale connections. Overall the teleconnection pattern in the tropical and Southern Pacific Ocean is well captured by the SST-forced ensemble, but it is absent or too weak in other oceanic areas. In the subtropical South Atlantic the correlation is more realistic in the coupled model experiment suggesting the importance of air-sea feedbacks for that region, even at lower than interannual timescales. When the composite analysis of SST and atmospheric fields is done only over the ensemble members having a PC1 in agreement with the observations, both in terms of sign and intensity, then the correspondence between model and data is much improved. The improvement relies on avoiding climate noise by averaging only over members that are statistically similar and it suggests a high level of uncertainty due to internal atmospheric variability. Some individual springs have been analyzed as well. In particular, 1982 represents a clean case with a clear wave train propagating from the central Pacific and merging with a secondary one from eastern tropical South Indian Ocean, and it corresponds to a strong El Nino. Another case, 2003, corresponds to a rainy spring for SESA but in this case the en-

51       semble mean does not exhibit any teleconnection through the South Pacific and it is  
52       not able to reproduce the correct local precipitation pattern, suggesting that in this  
53       case regional effects are more important than remote forcing.

## 54 **1 Introduction**

55 La Plata basin (LPB) is a region in South Eastern South America (SESA) comprising southern  
56 Brazil, Uruguay, northeastern Argentina, southern Paraguay and southern Bolivia that strongly  
57 relies on agriculture and hydro-electricity power. LPB region is a key area for the variability of  
58 the precipitation over South America having high values in all the seasons (see Zamboni et al.,  
59 2010). River discharge anomalies in SESA and analysis of precipitation regime over South Amer-  
60 ica evidence low frequency variability (Robertson and Mechoso, 2000; Berbery and Barros, 2002;  
61 Rusticucci and Penalba, 2000), but its nature is not fully understood yet. Different hypothesis have  
62 been discussed in recent decades, like the decadal changes in the ENSO-SAM correlation (Fogt  
63 and Bromwich, 2006), a possible influence of Pacific decadal variability (Barreiro, 2010), includ-  
64 ing the role of the 1976/77 North Pacific climate shift (Huang et al., 2005), the impact of tropical  
65 Atlantic SSTA, as the tropical component of the Atlantic Multidecadal Oscillation (AMO Seager  
66 et al., 2010). Throughout most of the last century, SESA experienced a trend toward increased  
67 precipitation (e.g. Barros et al., 2008) but it is likely that anthropogenic climate forcing may ex-  
68 plain only part of the wetting trend, as IPCC AR4 model simulations predict a weak increase in  
69 SESA precipitation over the last century (Seager et al., 2010).

70 At interannual timescales LPB precipitation has been linked to El Nino Southern Oscillation  
71 (ENSO) with a clear seasonality in the connection (Aceituno, 1988; Grimm et al., 2000; Paegle  
72 and Mo, 2002; Grimm, 2003; Cazes-Boezio et al., 2003; Vera et al., 2006; Barreiro, 2010, among  
73 others). El Nino influences SESA involving both upper and lower levels circulation anomalies:  
74 increased seasonal precipitation develops over LPB, while the northeast South America experi-  
75 ences drier conditions, and during La Nina the sign of the anomalies is reversed (Grimm et al.,  
76 2000). In the upper levels, Rossby wave trains propagating from the equatorial Pacific influence  
77 baroclinicity and advection of cyclonic vorticity over SESA (Yulaeva and Wallace, 1994; Grimm  
78 et al., 2000). In the lower levels, anomalous intensity and direction of the South American Low  
79 Level Jet (SALLJ) may change the moisture variability (Liebmann et al., 2004; Silvestri, 2004,  
80 i.e). The season with the best established teleconnection between ENSO and LPB hydro-climate  
81 is austral spring (Cazes-Boezio et al., 2003; Barreiro, 2010; Zamboni et al., 2011). Spring is also

82 the season corresponding to the largest influence of the Southern Annular Mode (SAM) on LPB  
83 precipitation (Silvestri and Vera, 2009). SAM is the leading mode of variability in the South-  
84 ern Hemisphere on low frequency. Positive (negative) SAM phase is associated with negative  
85 (positive) pressure anomalies over Antarctica and positive (negative) anomalies at middle lati-  
86 tudes (Thompson and Wallace, 2000). As a consequence of the SAM phase, decreased/increased  
87 precipitation over SESA is linked with weakened/enhanced moisture convergence associated with  
88 the anomaly of the upper level circulation over the southeastern Pacific Ocean (Silvestri and Vera,  
89 2003).

90 The efforts to explain SESA precipitation variability have been based on both observations and  
91 model analysis. The comparison of the IPCC AR4 coupled model performance in simulating  
92 SESA precipitation and its variability reveal that they have problems in representing accurately  
93 the variability associated with the South Atlantic Convergence Zone (SACZ), but models having  
94 a good ENSO tend also to have a good teleconnection in South America (e.g. Silvestri and Vera,  
95 2008; Vera and Silvestri, 2009). AGCM with forced SST have been tested as well analyzing pre-  
96 cipitation and circulation biases over SA (Zhou and Lau, 2002), investigating the remote forcing  
97 from different ocean basins for predictability issues (Barreiro, 2010), or assessing their ability to  
98 reproduce the past history of SESA precipitation (Seager et al., 2010). Nevertheless the causes  
99 of the present interannual and lower timescale variability of SESA precipitation remain not fully  
100 explained.

101 Tropical oceans SST could affect the climate of South America through different mechanisms  
102 like Rossby wave trains that propagate into the extra-tropics and then into South America, af-  
103 fecting its eastern regions (i.e. Paegle and Mo, 2002; Vera et al., 2004); shift and alteration of the  
104 Walker circulation (Cazes-Boezio et al., 2003); influence of subtropical jets and inflow of humidity  
105 southward (Byerle and Paegle, 2002). In the present study we intend to investigate the influence  
106 from remote forcing (i.e. mainly SST) following the mechanisms just described. In particular,  
107 the model performance of atmosphere-only and atmosphere-ocean coupled experiments is inves-  
108 tigated and compared in terms of hydro-climate variability over SESA at interannual and lower  
109 timescales. The analysis is mostly focused on austral spring when the connection between ENSO

110 and LPB precipitation is known and well established. A large ensemble of AMIP-type experi-  
111 ments with same boundary forcing (i.e. interannually varying SST) and different initial conditions  
112 is analyzed in terms of the correspondence between its PC1 and the data one. Some specific case  
113 studies have been considered as well.

114 The study is organized as follows: section 2 describes the model used and the experiments  
115 performed, including a list of the datasets and reanalysis used to verify the model performance.  
116 Section 3 is dedicated to the analysis of the hydro-climate variability (mainly in terms of precipi-  
117 tation variability) and its relationship with remote forcing. Section 4 investigates in more details  
118 the characteristics of the remote SST forcing over LPB precipitation, classifying years according  
119 to EOFs model performances. Section 5 lists and analyzes specific test cases. Finally, section 6  
120 summarizes the main conclusions of the study.

## 121 **2 Description of model experiments and datasets**

122 Two kinds of experiments have been used for the present study: an ensemble of AMIP-type experi-  
123 ments and a 20th century coupled model simulation. The ensemble of AMIP-type experiments  
124 consists of 9 members with same boundary conditions, which are interannually varying SST taken  
125 from the HadISST dataset (Rayner et al., 2003), and different initial conditions. The period ana-  
126 lyzed is 1948-2003. The experiments have been performed with the ECHAM4 atmospheric gen-  
127 eral circulation model (Roeckner et al., 1996) at T106 horizontal resolution (corresponding to a  
128 grid of  $1^\circ \times 1^\circ$ ) and 19 sigma vertical levels.

129 The twentieth century coupled model simulation (hereafter SSXX) has been performed with  
130 the fully coupled atmosphere-ocean general circulation model SINTEXG (Gualdi et al., 2008).  
131 This includes prescribed concentration of greenhouse gases (i.e. CO<sub>2</sub>, CH<sub>4</sub> N<sub>2</sub>O and chlorine-  
132 fluorocarbons) and sulfate aerosols, as specified for the 20C3M experiment defined for the IPCC  
133 AR4 simulations (see [http://www-pcmdi.llnl.gov/ipcc/about\\_ipcc.php](http://www-pcmdi.llnl.gov/ipcc/about_ipcc.php) for more details). The char-  
134 acteristics of both atmospheric and oceanic model components are described in previous publi-  
135 cations (Cherchi et al., 2008; Gualdi et al., 2008). The atmospheric component is the same used  
136 for the AMIP-type simulations. The oceanic component is OPA (Madec et al., 1998), which is

137 spatially distributed over a three-dimensional Arakawa-C-type grid (about  $2^\circ \times 2^\circ$  horizontal res-  
138 olution, with a meridional refinement of  $0.5^\circ$  at the Equator, and 31 prescribed vertical levels).

139 The model outputs have been compared with observations and re-analysis data. In particular, the  
140 global distribution of sea surface temperature has been taken from the HadISST dataset (Rayner  
141 et al., 2003), atmospheric fields come from the NCEP reanalysis (Kalnay et al, 1996), and the  
142 global precipitation over land is taken from the CRU dataset (Mitchell and Jones, 2005). Satellite  
143 globally distributed precipitation for the period 1979-2003 from the CMAP dataset (Xie and Arkin,  
144 1997) has been used for comparison with and validation of the land-precipitation dataset.

### 145 **3 Simulated hydro-climate variability over South America**

146 The analysis in this section focuses on the hydro-climate variability (mostly based on precipita-  
147 tion) over South America with emphasis on its southeastern part during austral spring (October,  
148 November, December mean; hereafter OND mean). Spring is chosen for our analysis because it  
149 has the largest teleconnection with ENSO (Grimm et al., 2000; Barreiro, 2010) and the largest  
150 correlation between observed and modeled LPB precipitation (not shown). Table 1 shows OND  
151 mean precipitation and its standard deviation averaged over South America and over LPB for the  
152 CRU dataset and for the model outputs. In the AMIP-type ensemble, the computation is applied  
153 to all the members as a single timeserie. In the LPB region the model simulates a larger than  
154 observed amount of precipitation, but its standard deviation is smaller (Table 1). That is to say that  
155 the model tends to underestimate the variability of the precipitation over SESA, even if it tends to  
156 overestimates its total amount.

157 In the literature precipitation variability over SESA, and over the LPB region in particular, has  
158 been measured by rainfall indices defined as averages over specific region (Boullanger et al., 2005;  
159 Vera and Silvestri, 2009; Barreiro, 2010, among others). Following Barreiro (2010), we define  
160 an LPB index as the averaged precipitation in the region  $37^\circ\text{S}-19^\circ\text{S}$ ,  $65^\circ-47^\circ\text{W}$  (over land points  
161 only). The region corresponds to the same area used to compute the LPB values in Table 1. In the  
162 AMIP-type ensemble mean that index, averaged in austral spring (OND), is significantly correlated  
163 with the analogue computed from CRU data (the correlation coefficient is 0.56), suggesting that

164 in this season the role of the forcing from oceanic SST is large. When the LPB index is filtered  
165 using a 7-years filter to keep the frequencies lower than 7 years (i.e. lower than interannual)  
166 the correlation is still significant and large (i.e. the value is 0.46). Even if in both cases a large  
167 component of internal variability remains (see Zamboni et al., 2011, for the interannual timescale)  
168 our study intends to focus on the forced one.

169 Because of the model weakness in simulating the intensity of precipitation standard deviation,  
170 we decided to identify an index based on the EOFs of the precipitation anomalies over South  
171 America. EOFs and PCs allow identifying the dominant modes of variability avoiding the in-  
172 consistencies between model and observations in the geographical differences. In past literature  
173 the dominant mode of variability of the precipitation over South America have been investigated  
174 using different datasets. Due to the sparse distribution of the observations in many regions of  
175 South America, gridded datasets, as e.g. the CRU dataset, cannot represent correctly its precip-  
176 itation (Stuck et al., 2006; Carril et al., 2012), and the global precipitation coverage taken from  
177 satellite measurements after 1979 (CMAP) is eventually more reliable. Nevertheless, over LPB  
178 region mean fields and variances of CRU and CMAP are very similar (Boulangier et al., 2005). We  
179 strengthen this result by comparing EOF patterns obtained from the two datasets.

180 Fig. 1 shows the first three EOFs of land precipitation over South America (between 45S and  
181 the Equator) during spring for the CRU and CMAP dataset during the overlapping period (1979-  
182 2005). It is possible to identify similar spatial patterns between them (fig. 1), in particular the  
183 north-south dipole depicted by the first mode and the triple pattern defining the third mode. In  
184 terms of temporal variability the PCs corresponding to the three leading EOFs are compared via  
185 correlation analysis (see Table 2): the correlation coefficients are large and statistical significant  
186 for the same PC (the diagonal in Table 2). These results suggest that in both datasets the modes  
187 are well separated. The results just discussed give us confidence in continuing the investigation  
188 using the CRU dataset, using the 50 years available to validate and compare the model results in  
189 the period 1948-2003.

190 Fig. 2 shows the first three modes of variability of South America precipitation during OND, and  
191 its principal components for the CRU dataset, but considering the long time record (1948-2003).

192 The dominant mode of variability is a north-south dipole with centers at 15S and 30S (fig. 2a) in  
193 the eastern part of the continent. Its first principal component (PC1, fig. 2b) corresponds to the  
194 variability of ENSO, as the correlation coefficient between PC1 and NINO3.4 (monthly mean SST  
195 anomalies averaged in the box 5S-5N, 170W-120W) is 0.59. The second pattern has three poles  
196 centered at 5S, 20S and 35S (fig. 2c), and the associated PC2 (fig. 2d) corresponds to decadal  
197 timescale variability. Finally, the third mode is an east-west dipole with centers between 15-  
198 20S (fig. 2e) and its PC (fig. 2f) corresponds to a trend, at least in the last part of the record.  
199 The comparison between the spatial patterns in fig. 2 and fig. 1 evidences that changing the time  
200 record length the first mode is unchanged, while the second and third one seem to be inverted. The  
201 difference could be related with the modulation of the decadal variability of LPB precipitation  
202 associated with the Southern Hemisphere climate, as discussed by Silvestri and Vera (2009).

203 The performance of the model in reproducing the dominant modes of variability of the precip-  
204 itation over South America is shown in fig. 3. In terms of spatial patterns the model is able to  
205 realistically represent the dominant modes of variability of the precipitation over South America.  
206 In fact, the first mode produced by the AMIP-type experiments is a north-south dipole with cen-  
207 ters over the LPB region and over the northeast part of the continent (fig. 3a). As second and third  
208 mode the patterns have centers forming a triple (fig. 3b) and an east-west dipole (not shown), re-  
209 spectively. In the AMIP-type ensemble the EOFs are computed over all the members concatenated  
210 to form a long record. Even in the coupled model the spatial patterns of the first two modes of  
211 variability are realistic (not shown). Table 3 summarizes the relationship between the principal  
212 components in the AMIP-type ensemble and ENSO: both PC1 and PC2 are significantly corre-  
213 lated with ENSO (i.e. NINO3.4 index). The latter is found for the AMIP-type experiment and not  
214 in the corresponding analysis using the coupled model experiment data.

215 On the base of these results we select the OND PC1 as index of precipitation variability over  
216 LPB. In particular, positive (negative) values correspond to wet (dry) conditions over LPB and dry  
217 (wet) ones to the north, following the intensity of the SACZ (Paegle and Mo, 2002; Silva et al.,  
218 2009; Liebmann et al., 2004). The correspondence between precipitation variability in LPB and  
219 remote SST during spring is shown in figure 4. The correlation coefficients between PC1 and

220 global SST identify the patterns related to ENSO and its teleconnections (fig. 4a). In fact, wet  
221 (dry) LPB years are related to positive (negative) SST anomalies in the Tropical Pacific and Indian  
222 Oceans, eastern equatorial Atlantic, subtropical South Atlantic near the South American coast and  
223 south eastern Pacific (with a max at 50S), and with negative (positive) SST anomalies in the central  
224 North Pacific, subtropical south western Pacific and southwestern South Atlantic (see also Paegle  
225 and Mo, 2002; Seager et al., 2010).

226 The ENSO-LPB precipitation teleconnection is strong and robust in the AMIP-type ensemble,  
227 even if with some biases. In particular, the pattern in the Pacific Ocean (from the tropical sector  
228 to its southern part) is well represented in the ensemble in agreement with the idea of its strong  
229 forced influence (fig. 4b). Concerning the other oceanic sectors, the teleconnection is absent in the  
230 North Pacific and in the sub-tropical South Atlantic and it is weaker in the Indian sector (fig. 4b).  
231 It is now well recognized that some patterns of SST variability result from a combination of atmo-  
232 spheric and oceanic processes (Deser et al., 2010). In the Indian Ocean the weakness in the model  
233 may be ascribed to the missed coupling in this set of experiments that is known to be important for  
234 the region (Bracco et al., 2007). The lack of the ocean-atmosphere coupling may be an explanation  
235 also for the performance in the subtropical South Atlantic, in agreement with Barreiro (2010). In  
236 fact, when the same analysis is conducted using the coupled model data the correlation in that re-  
237 gion is more realistic (fig. 4c). Over the Indian Ocean the bias is not improved despite the presence  
238 of the ocean-atmosphere feedback (the values are in fact weaker than observed even in fig. 4c).  
239 Moreover, in the tropical Pacific Ocean the correlation tends to extend for the whole basin (up  
240 to the western edge) and this is consistent with the well-known biases of the model in the ENSO  
241 representation (Navarra et al., 2008). In the North Pacific the model misses the right connection  
242 with ENSO as it is wrongly triggered by model biases and air-sea coupling influences (Cherchi  
243 et al., 2011).

244 Considering timescales lower than interannual, we applied a 7 years low pass filter to the PC1  
245 and then we computed the time-correlation with the SST. The results indicate that at low frequen-  
246 cies there are no indication of relevant patterns identifying a link between SST and precipitation  
247 in LPB (fig. 5). In the observations, positive significant values are found in the south Pacific sector

248 (50S, 150W) and in the tropical north Atlantic (fig. 5a). In the model the positive correlation in the  
249 south Pacific sector is captured, while the signal in the north Atlantic sector is missing (fig. 5b).  
250 Additionally, in the AMIP-type ensemble there is a spurious negative correlation in the western  
251 sectors of both Pacific and Equatorial Atlantic Oceans (fig. 5b). On the other hand in the coupled  
252 model the correlation tends to be weaker everywhere (fig. 5c). Overall, the model has difficulties  
253 in capturing variability at frequency lower than interannual. In the case of the AMIP-type ensem-  
254 ble this may suggest that the internal variability could represent an important component of these  
255 modes.

256 Another remote forcing for the precipitation in the LPB region comes from the Southern An-  
257 nular Mode (SAM; Thompson and Wallace, 2000). SAM depends on the interactions between  
258 the tropospheric jet stream and extratropical weather systems, being a source of uncertainty for  
259 the simulated climate at mid- to high southern latitudes (Deser et al., 2012). It has signatures in  
260 the tropospheric circulation and midlatitudes storm tracks and therefore could affect weather in  
261 southern South America (Menéndez and Carril, 2010), but its influence on SESA precipitation  
262 was not stable over recent decades (Silvestri and Vera, 2009). For the observations, our SAM  
263 index is based on in situ sea level pressure (Marshall, 2003) and it is taken from [http://www.nerc-](http://www.nerc-bas.ac.uk/icd/gjma/sam.html)  
264 [bas.ac.uk/icd/gjma/sam.html](http://www.nerc-bas.ac.uk/icd/gjma/sam.html) as OND mean. For the model it is defined as difference of zonal  
265 mean sea level pressure between 40S and 65S, following Marshall (2003). Fig. 6 shows a sliding  
266 correlation on 19 years between this index and the LPB precipitation index defined before (i.e. in  
267 Table 1). The magenta solid line of fig. 6 indicates that the correlation between the two indices  
268 is non-significant up to mid-70s, and then it becomes significant and negative. In fact, the time  
269 regression of the SAM index and the precipitation has a strong dipole signature only after 1979,  
270 while before the signal is weak (not shown).

271 In the AMIP-type ensemble the same analysis is conducted but considering the correlation of  
272 the ensemble mean (fig. 6, black solid line) and the mean of the correlation in each member (fig. 6,  
273 dashed black line). The distinction is motivated by the idea of identifying and discussing the forced  
274 and internal variability components. The correlation of the ensemble mean shows a change to a  
275 negative and significant correlation after mid-70s, suggesting that the change contain a component

276 that is forced by the SST. On the other hand, the mean of the correlation for each member is never  
277 significant suggesting that either the model is not able to reproduce the correct internal variability,  
278 or that its role is not dominant in this case. Considering the ensemble mean, a weakening of the  
279 time regression pattern between SAM and precipitation in the LPB region is simulated even if it  
280 is not as pronounced as observed (not shown).

#### 281 **4 Remote forcing on LPB precipitation variability**

282 We classified wet (dry) LPB years using the first principal component (PC1) of precipitation  
283 anomalies over South America (as defined in the previous section), choosing 1 (-1) standard devi-  
284 ation as threshold. Wet (dry) LPB years correspond to precipitation dipoles with excess (deficit)  
285 of precipitation over LPB and the reverse north of it, respectively (fig. 3a).

286 Fig. 7 shows composite of SST and 200 mb eddy streamfunction for wet and dry LPB years  
287 computed for the HadISST/NCEP datasets and for the AMIP-type ensemble. In the observations,  
288 the SST anomalies are almost symmetric between the two phases in the tropical and south extra-  
289 tropical Pacific, but not in the extra-tropical North Pacific, in the Indian Ocean and in the sub-  
290 tropical South Atlantic sectors (fig. 7a,b). In particular, wet LPB years are associated with positive  
291 SST anomalies remarkably large over the eastern tropical Pacific (Zhou and Lau, 2001; Paegle  
292 and Mo, 2002; Seager et al., 2010), but also significant over the western tropical Indian Ocean and  
293 the eastern tropical Atlantic Ocean (i.e. the Gulf of Guinea). Furthermore, wet LPB years have  
294 negative SST anomalies in the western subtropical south Pacific, and partially in the eastern side of  
295 the Indian Ocean. The SST patterns with warm tropical Pacific and cold subtropical South Pacific  
296 enhances the convection in the SPCZ southeastward into the subtropical regions, and intensifies  
297 localized overturning cells associated with an anomalous Rossby wave source in the central south  
298 Pacific convergence zone (Vera et al., 2004). During dry LPB years SST anomalies of opposite  
299 sign are found over tropical southern Pacific and in the Indian Ocean, although the latter are less  
300 pronounced. Similar anomalies to those corresponding to the wet years are observed over the  
301 extratropical North Pacific while negative anomalies exist in the subtropical South Atlantic, off  
302 the South American coast (fig. 7a,b).

303 In the AMIP-type ensemble, when the composite is built considering the PC1 of all members,  
304 SST anomalies are realistic in the tropical and southern Pacific Ocean but not in the North Pacific,  
305 Tropical Indian and Atlantic sectors (fig. 7c,d). In particular, the asymmetry between strong and  
306 weak LPB years in the North Pacific is not simulated, and the anomalies in the Indian sector are  
307 largely weaker than observed.

308 In the observations, in both wet and dry LPB years, there is a wave train propagating from the  
309 western Pacific/Indian sector, as depicted by the 200 mb eddy streamfunction (fig. 7a,b contours),  
310 it recalls the Pacific South American Mode (Mo and Paegle, 2001; Chan et al., 2008; Taschetto  
311 and Ambrizzi, 2012). These patterns are remarkably symmetric in the Southern Hemisphere,  
312 while the signal north of the Equator in the Asian sector is larger during wet LPB years (fig. 7a,b).  
313 During wet LPB years the intensities are larger in the starting propagating phase, but in the dry  
314 LPB years the positive streamfunction anomalies over SESA and adjacent Atlantic sector are more  
315 intense. Vera et al. (2004) and Zamboni et al. (2012) proposed that these may originate from the  
316 central Pacific, but the amplification may also arise from local processes over SESA.

317 In the model anomalies recalling the PSA can be identified (fig. 7c,d) with the contribution from  
318 the central Pacific being more evident. During dry LPB years, in the coupled model SST anomalies  
319 in the subtropical south Atlantic, off the South American coast, are negative as in the observations,  
320 suggesting that the ocean-atmosphere coupling for this sector is important (not shown).

321 In the AMIP-type ensemble, the model PC1 for each member may peak in the same years as in  
322 the observations but also in others. We found that composing years according to the correspon-  
323 dence between AMIP-type PC1 and observed PC1 provides some extra information on the origin  
324 of the remote SST forcing for the LPB hydro-climate. We have classified years as "In Phase" when  
325 the model PC1 exceed 1 standard deviation (std) as in the observations, as "Out of Phase" when  
326 the model PC1 is of opposite sign as the observed one and as "Partial In Phase" when the model  
327 PC1 has the same sign as the observed one but the former does not exceed 1 std. During the "Out  
328 of Phase" years, the precipitation composites have excess (deficit) of precipitation in the region  
329 north of the La Plata Basin without any clear signal in the southern part of the dipole (not shown).  
330 During "In Phase" years the dipole structure is the strongest, while it is almost destroyed during

331 "Partial in Phase" years. However, in the latter case the anomalies over LPB, even if weaker, are  
332 of the same sign as in the "In Phase" group (not shown).

333 It is instructive to discuss the composite of SST and 200 mb eddy streamfunction built using  
334 the classification just introduced (fig. 8). The "In Phase" composite of SST (fig. 8a,b) reflects the  
335 observed anomalies (fig. 7a,b). In fact, during wet LPB years positive anomalies in the central  
336 eastern Pacific are associated with positive anomalies in the Indian sector and negative anomalies  
337 in the subtropical south Pacific. On the other hand, during dry LPB years negative anomalies in  
338 the central eastern Pacific are associated with positive anomalies in the North Pacific and negative  
339 anomalies in the South Atlantic (around 30S), off the SA coast. A main difference exists in the  
340 subtropical Indian sector where the In Phase composite has anomalies near zero and not negative  
341 as in the observations.

342 The comparison between fig. 7 and fig. 8 suggest that the forcing from SSTA in the tropical  
343 Pacific Ocean may provide both wet and dry conditions in the LPB region and that the forcing  
344 from other basins, like the Atlantic and the Indian Oceans, may trigger the teleconnection with  
345 the Pacific. In fact, in the "Out of Phase" composite (fig. 8c,d) the SST anomalies in the tropical  
346 Pacific and Indian Ocean sectors corresponds to the "In Phase" composite, while the anomalies in  
347 the North and subtropical South Pacific and in the Atlantic region largely differ. On the other hand,  
348 the main differences between "In Phase" and "Partial In Phase" composites in terms of SST are  
349 localized in the Indian Ocean (fig. 8e,f). The comparison between "In Phase" and "Out of Phase"  
350 composites suggests that an SST pattern with negative (positive) anomalies south west of large  
351 positive (negative) anomalies in the tropical Pacific Ocean may have a dominant role in terms of  
352 the wave propagation of the atmospheric teleconnection from the Indian-Pacific sector to South  
353 America (Vera et al., 2004; Zamboni et al., 2012).

354 Similarly to the SST, the wave propagation in the "In Phase" composite corresponds to the  
355 observations (fig. 8a,b) for both wet and dry LPB years with a clear wave train propagating from  
356 west to east. In the positive case, positive SST anomalies in the central eastern Tropical Pacific  
357 are associated with positive anomalies in the Indian sector and with negative anomalies in the  
358 subtropical south Pacific in correspondence of the dateline. Both the conditions are present only

359 when the "In Phase" positive cases are considered, and they seem both responsible of the wave  
360 train. In the negative case, the HadISST composite has an SST pattern just opposite, but with  
361 the negative anomalies in the Indian Ocean weaker (considering their absolute values) than in  
362 the positive case. Further, in the "In Phase" negative composite the values in the Indian Ocean  
363 are near zero. Actually in this last case the wave train seems to propagate from Indonesia rather  
364 than from the eastern Indian sector as in the positive case. However we may not either exclude  
365 the possibility that they correspond to a positive interference of two wave trains (Zamboni et al.,  
366 2012). Further comparing fig. 7 and fig. 8 evidences that the "Out of Phase" composite does not  
367 have any propagating signals (fig. 8c,d), while the "Partial in Phase" one has a wave train weaker.  
368 Further, it seems to propagate from the Indian (central Pacific) sector in the positive (negative)  
369 case (fig. 8e,f).

370 Shift and alteration of the Walker circulation associated with SSTA in the tropical oceans di-  
371 rectly affect tropical South America (Cazes-Boezio et al., 2003). During warm ENSO events the  
372 Walker circulation shifts eastward and its subsiding branch occurs over South America. When the  
373 dipole is in its positive phase, i.e. rainy SESA and dry Amazon, subsidence over the Amazon is  
374 particularly evident for the "In Phase" composite, as shown from its mean vertical velocity (see  
375 Table 4). Conversely, when the dipole is in its negative phase the vertical velocity anomaly has  
376 the opposite sign, favoring convection over northern South America (Table 4). In terms of local  
377 processes over South America, the "In Phase" composite of vertically (from the surface to about  
378 200 mb) integrated moisture shows a well-defined dipole between SESA and Amazon (fig. 9a,b).  
379 The anomalies are symmetric comparing positive and negative phases, and the moisture fluxes are  
380 directed north-easterly (south-westerly) in correspondence of positive (negative) moisture anoma-  
381 lies (fig. 9a,b). The "Out of Phase" composite shows fluxes directed in the opposite direction and  
382 the moisture anomalies over SESA are absent or extremely weak (fig. 9c,d). In the latter case,  
383 anomalies of sign opposite to the "In Phase" composite are large in the northern part of South  
384 America (fig. 9c,d).

385 During warm ENSO events, stronger upper tropospheric subtropical westerlies over the Andes  
386 correlate with an eastward and southward humidity flow emanating from the Amazon basin to-

ward LPB (Byerle and Paegle, 2002). Regarding the anomalies in the westerlies over the Andes near the position of the subtropical jet (last column of Table 4), stronger upper tropospheric, subtropical westerlies over the Andes (e.g. during warm ENSO events) correlate with an eastward and southward humidity flow emanating from the Amazon basin toward LPB (Byerle and Paegle, 2002). Indeed, the positive phase of the dipole (rainy SESA) coincides with an intensification of the westerlies, suggesting a larger moisture supply from the northwest through the low-level jet. The weakening of the subtropical jet in the negative phase suggests opposing processes.

## 5 Some case studies

Table 5 summarizes the results from the AMIP-type ensemble in terms of the classification into "In Phase" and "Out of Phase" groups. In particular it contains the number of members of the ensemble in agreement with CRU results, as a measure of the inter-ensemble spread. For positive PC1 cases (i.e. wet LPB years), 1982 and 2003 represent two interesting cases worth of further investigation. In particular, 1982 is the only case having all the nine members reproducing the observed result: 100% of the members have a positive PC1 exceeding 1 standard deviation as in the observations. This case could be interpreted as the clean example of remote SST influence; moreover it corresponds to one of the strongest El Nino years in the analyzed record. Year 2003 is characterized by having 8 members over 9 with a negative large PC1 (exceeding -1 standard deviation) rather than a positive large one as in the CRU dataset.

As we mentioned in section 3, in the observations the correlation between PC1 and NINO3.4 is significant. When we consider OND SA precipitation PC1 years exceeding 1 (-1) std, 3 over 7 (2 over 8) wet (dry) LPB years correspond to El Nino (La Nina) event. This means that only 3(2) over 7(8) extreme wet (dry) LPB years occurred in correspondence of an El Nino (La Nina) year. However, as the teleconnection from the Pacific to the South America is almost simultaneous, the SSTA in October-November may have large impact even if they may not develop into ENSO years (Zamboni et al., 2012).

For negative PC1 cases (i.e. dry LPB years) it is hard to identify a net common behavior among the members. We decided to focus on 1999 because in the model it has 4 members "In Phase" and

414 5 members "Partial In Phase" with CRU results, and it corresponds to a La Nina year.

#### 415 5.1 1982 case study

416 Year 1982 is the only case in our record having all the members with a PC1 larger than 1 std  
417 as in the observations: as all the members agree, we expect that the LPB precipitation pattern is  
418 completely forced from remote SST distribution. Fig. 10b shows the precipitation pattern in the  
419 AMIP-type ensemble composite (merging all 1982 years) with a well-defined dipole with excess  
420 of precipitation over LPB and deficit north of it, associated with a low-level convergence. In  
421 terms of SST, 1982 represents one of the strongest El Nino in the recent record with large positive  
422 SSTA in the eastern tropical Pacific Ocean (fig. 10a). During that year, positive SSTA in the  
423 tropical Pacific region are associated with negative SSTA in the subtropical Pacific around the  
424 dateline (both north and South of the Equator), weak positive anomalies in the Western Indian  
425 Ocean and negative anomalies in the Equatorial and subtropical South Atlantic. In the model, this  
426 SST pattern produces a clean wave train propagating from the central Pacific and merging with  
427 a secondary one from eastern tropical South Indian Ocean (fig. 10a). Over South America, the  
428 200 mb streamfunction north of 20S is positive, in agreement with the observations (not shown),  
429 while it is negative (positive) south of it in the east (west), differently from the observations (not  
430 shown). In this case, the simulated precipitation anomalies over LPB can be interpreted as a net  
431 consequence of the teleconnection from the Pacific-Indian Ocean sectors.

#### 432 5.2 2003 case study

433 During 2003, considering the reanalysis datasets, wet conditions over LPB are basically explained  
434 by a wave 3 configuration (fig. 11a), rather than from a teleconnection from the Pacific. 2003 is not  
435 an El Nino year and it experienced SST anomalies generally warmer than the mean climatology in  
436 all the tropical basins (fig. 11a,c). In this case the dipole precipitation pattern over South America  
437 seems to be mostly related to local effects rather than to remote SST forcing.

438 In the AMIP-type ensemble, the wave-3 pattern is not simulated (fig. 11c, contours) and the  
439 200 mb streamfunction standard deviation ((fig. 11d) shows large spread among members in the  
440 Southern part of South America. Over LPB, as indicated by the sign of PC1, precipitation is

441 mostly negative (fig. 11d). Large positive SSTA, mainly in the Atlantic, are associated with intense  
442 precipitation north of 30S (fig. 11d): large positive precipitation anomalies over Amazon and  
443 slightly negative values over LPB provide a negative PC1, i.e. in this case "Out of Phase" than  
444 observed.

445 Eddy streamfunction at 200 mb is highly variable among the members and only one over nine is  
446 able to reproduce the wave-3 pattern (fig. 12). In this case the internal variability and the associated  
447 spread among the ensemble members dominate the model simulation of hydro-climate over LPB  
448 and the remote SST forcing is less efficient.

### 449 5.3 1999 case study

450 Year 1999 experienced a strong La Nina with large negative SSTA in the tropical central and  
451 eastern Pacific Ocean (fig. 13a,c). Over South America dry (wet) conditions occur over LPB  
452 (north of it) (fig. 13b). In the model ensemble, four and five members have a PC1 "In Phase" and  
453 "Partial In Phase", respectively, with the CRU PC1. The model composite of these members shows  
454 negative precipitation over LPB and positive anomalies north of 20S (fig. 13d), but the values  
455 are weaker than observed (fig. 13b). In terms of teleconnection patterns, positive streamfunction  
456 anomalies in the upper troposphere are related with a quadruple between western Pacific and  
457 American continent sectors (fig. 13a). In the model the anomalies over SESA are largely weaker  
458 than observed (fig. 13c) and to verify the inter-ensemble performance we consider all the members  
459 separated.

460 Fig. 14 shows precipitation and 200 mb eddy streamfunction anomalies during OND for each  
461 member and for the ensemble mean. The members with a clear dipole with negative precipitation  
462 anomalies over LPB have positive 200 mb eddy streamfunction anomalies over SESA associated  
463 with a quadruple between western Pacific and American continent sectors (fig. 14b, g,h,i). In these  
464 cases an internal variability component dominates (fig. 13e), as the SST pattern is the same also  
465 for the other members.

## 466 **6 Conclusions**

467 We studied the influence from tropical SST anomalies on the precipitation variability over SESA at  
468 interannual and at lower than interannual timescales. The focus has been placed on the evaluation  
469 and analysis of ensemble continuous 1948-2003 integrations performed with an atmospheric GCM  
470 with relatively high horizontal resolution (1x1). It was also used a coupled global model to explore  
471 the potential importance of ocean-atmosphere interaction. We focus on the study of the austral  
472 spring motivated by the fact that during this season the signal from the tropical Pacific is more  
473 robust (e.g. Grimm et al., 2000; Barreiro, 2010).

474 Relatively high level of uncertainty in the observations characterizes large areas of South Amer-  
475 ica (Carril et al., 2012). However, our results indicate that the regional climate modes of variabil-  
476 ity calculated from two independent precipitation databases (CRU and CMAP) for 1979-2003 are  
477 similar. Therefore we assume that CRU precipitation for the period 1948-2003 is realistic enough  
478 and we can use it for the purpose of model evaluation of broad scale regional modes of variability  
479 during austral spring.

480 In terms of seasonal area mean precipitation over SESA and its standard deviation, both atmo-  
481 spheric and coupled models made a good performance, with the seasonal mean slightly overesti-  
482 mated and its variability somewhat underestimated. The analogue computed from observations is  
483 significantly correlated with the values obtained from the SST-forced ensemble, suggesting that  
484 oceans influence the precipitation over SESA.

485 Both the atmospheric and the coupled models realistically capture the spatial patterns of the two  
486 dominant precipitation modes of variability over South America. The first mode is a south-north  
487 precipitation anomaly dipole with centers over SESA and central-northern Brazil and its principal  
488 component is used as a climate index of precipitation interannual variability (PC1). Its correlation  
489 with global SST identifies the patterns related to ENSO and its teleconnections. The teleconnec-  
490 tion pattern in the southern Pacific Ocean is well captured in the SST-forced ensemble, but it is  
491 absent or too weak in other oceanic areas. The correlation in the subtropical South Atlantic is more  
492 realistic in the coupled model experiment, suggesting that air-sea feedbacks would be important  
493 there. These correlations with the SST were also calculated for time scales lower than interan-

494 nual for which the filtered (7-year low-pass filter) first PC of precipitation over South America has  
495 been used as an index. The atmospheric model tends to capture qualitatively well the pattern of  
496 lower-frequency teleconnections over vast areas of the Pacific, but tends to fail over the Atlantic.  
497 Correlations tend to be too weak in the coupled model. However, its performance is qualitatively  
498 acceptable in the south Atlantic again suggesting the potential importance of ocean-atmosphere  
499 interactions in this sector.

500 The analysis of the relationship between SAM and LPB hydro-climate reveals that even though  
501 the annular mode is associated with internal atmospheric variability, there is hint to a possible  
502 oceanic influence on SAM variability on decadal timescales. The long-term time evolution of the  
503 correlation between the SAM index and the precipitation in SESA was evaluated in a way to dis-  
504 tinguish the forced variability (correlation of the ensemble mean) from the internal atmospheric  
505 variability or climate noise (the average correlation of each member). During the last decades  
506 the positive phase of the SAM is associated with decreased precipitation over SESA for the ob-  
507 servations (consistent with Silvestri and Vera, 2009). In particular, we found that the SST-forced  
508 variability resembles the evolution of the observed correlations, while the internal variability does  
509 not, suggesting a potential for the SST anomalies to influence on the spatial circulation anomaly  
510 patterns typically associated with the SAM.

511 Composite fields of upper-tropospheric streamfunction anomalies averaged over all the wet  
512 springs in SESA consist in wave trains extending southeastward from eastern Indian Ocean and  
513 Indonesia before they turn equatorward into South America. The dry composite is almost sym-  
514 metric in the tropical and southern Pacific. These wave trains share some elements of the second  
515 and third leading modes of SH circulation variability on interannual time scales (e.g. Mo, 2000,  
516 the first leading mode of SH circulation variability is the SAM). The SST-forced ensemble cap-  
517 tures the circulation anomalies and also those of SST in the tropical and southern Pacific, but the  
518 anomalies are of lower amplitude than observed. Interestingly, the atmospheric model does not  
519 capture the cold anomaly in the subtropical South Atlantic for the dry composite, but the coupled  
520 model does, further confirming the importance of ocean-atmosphere interaction in this sector.

521 If the composite for wet/dry events is done by averaging only over those ensemble members

522 for whom the model and observations agree regarding the occurrence of strong positive/negative  
523 precipitation anomalies ("In Phase" composite), then the structure of teleconnections corresponds  
524 better with the observed. This improvement arises from avoiding the climate noise by averaging  
525 only over members that are statistically similar on the basis of the principal component of the  
526 leading precipitation mode over South America. The SST anomaly in the Indian Ocean (correctly  
527 captured in the "In Phase" composite) seems to be a factor to take into account since it is in this  
528 sector where the wave train influencing the precipitation dipole in South America originates. The  
529 pathway from the tropical Indian Ocean would be particularly important in spring as in this season  
530 there is strong covariation of ENSO and the Indian Ocean dipole (Cai et al., 2011).

531 We analyzed some individual springs for which the number of ensemble members in agreement  
532 with observations was very different (regarding the first leading mode of precipitation variability  
533 in South America). In the 1982 spring all members coincide in the rainfall anomaly dipole as  
534 observed. In this case the enhanced northerly low-level flow and moisture transport to the east of  
535 the Andes feed convection over SESA. The associated SST pattern produces a clean wave train  
536 propagating from the central Pacific and merging with a secondary one from eastern tropical South  
537 Indian Ocean. In 1982 occurred a strong El Nino event. However, for other El Nino or La Nina  
538 events (e.g. 1987 or 1999) the agreement between the ensemble members for simulating the rain-  
539 fall dipole was not as good as in 1982, at least in part associated with unclear teleconnections (i.e.  
540 large dispersion between simulated members). It is also worth noting that only some "extreme"  
541 springs (i.e. too rainy or too dry in SESA in terms of PC1 index) are associated with the occurrence  
542 of El Nino or La Nina.

543 A rainy spring for SESA was 2003, but in this case almost all the ensemble members exhibit  
544 a precipitation dipole out of phase with respect to the observations (from this point of view is  
545 an opposite case to 1982). This year exhibits a zonally symmetric pattern of moderately positive  
546 SST anomalies throughout the tropics. In particular, near neutral conditions dominate across the  
547 equatorial Pacific. In this case, the ensemble mean does not exhibit any teleconnection through  
548 the South Pacific. Not having sectors with high temperature anomalies in the tropics is a source  
549 of additional uncertainty in the simulation of the SH extratropics since wave trains propagating

550 through the Southern Oceans are not excited uniformly in the different ensemble members (large  
551 inter-member spread in the circulation). Regional effects would be more important than remote  
552 forcing in this case.

553 In terms of intensity it is hard to separate from the analysis we did the influence of the strongest  
554 cases chosen. Further about the conclusions of the Indian Ocean we may not exclude that its  
555 variability is also induced by ENSO.

556 *Acknowledgements.* The research leading to these results has received funding from the European Com-  
557 munity's Seventh Framework Programme (FP7/2007-2013) under Grant Agreement N° 212492 (CLARIS  
558 LPB. A Europe-South America Network for Climate Change Assessment and Impact Studies in La Plata  
559 Basin). A. F. Carril and C. G. Menéndez were partially supported by PIP 112-200801-01788 (CONICET,  
560 Argentina) and PICT 2008-00237 (FONCYT, Argentina). The support of Italian Ministry of Education,  
561 University and Research, and Ministry for Environment, Land and Sea through the project GEMINA is  
562 gratefully acknowledged as well. Dr. L. Zamboni was partially supported by American Recovery and  
563 Reinvestment Act (ARRA) funding through the Office of Advanced Scientific Computing Research, Office  
564 of Science, U.S. Dept. of Energy, under Contract DE-AC02-06CH11357 and by the U.S. Department of  
565 Energy, Basic Energy Sciences, Office of Science, under contract # DE-AC02-06CH11357.

566 **References**

- 567 Aceituno P (1988) On the functioning of the Southern Oscillation in the South American sector. Part I:  
568 Surface climate. *Mon Wea Rev*, 116, 505-524
- 569 Barreiro M (2010) Influence of ENSO and the South Atlantic Ocean on climate predictability over south-  
570 eastern South America. *Clim Dyn*, 35, 1493–1508 DOI:10.1007/s00382-009-0666-9
- 571 Barros VR, Doyle ME, Camilloni IA (2008) Precipitation trends in southeastern South America: Relation-  
572 ship with ENSO phases and with low-level circulation. *Theor Appl Climatol*, 93, 19-33
- 573 Berbery EH, Barros VR (2002) The hydrologic cycle of the La Plata basin in South America. *J Hydromet*  
574 3: 630–645
- 575 Boulanger JP, J Leloup, O Penalba, M Rusticucci, F Lafon, W Vargas (2005) Observed precipitation in the  
576 Parana-Plata hydrological basin: long-term trends, extreme conditions and ENSO teleconnections. *Clim*  
577 *Dyn* 24: 393–413
- 578 Bracco A, Kucharski F, Molteni F, Hazeleger W, Severijns C (2007) A recipe for simulating the interannual  
579 variability of the Asian summer monsoon and its relation with ENSO. *Clim Dyn* 28: 441–460
- 580 Byerle LA, Pagle J (2002) Description of the seasonal cycle of low-level flows flanking the Andes and their  
581 interannual variability. *Meteorol* 27: 71–88
- 582 Cai W, van Rensch P, Cowan T, Hendon HH (2011) Teleconnection pathways of ENSO and the IOD and  
583 the mechanisms for impacts on Australian rainfall. *J Clim* 24: 3910–3923
- 584 Carril AF, and co-authors (2012) Performance of a multi-RCM ensemble for South Eastern South America.  
585 *Clim Dyn* (under revision)
- 586 Cazes-Boezio G, Robertson AW, Mechoso CR (2003) Seasonal dependence of ENSO teleconnections over  
587 South America and relationships with precipitation in Uruguay. *J Climate*, 16, 1159-1176
- 588 Chan SC, Behera SK, Yamagata T (2008) Indian Ocean dipole influence on south American rainfall. *Geo-*  
589 *phys Res Lett* 35 L14S12 doi:10.1029/2008GL034204
- 590 Cherchi A, Masina S and Navarra A (2011) Tropical Pacific-North Pacific teleconnection in a coupled  
591 GCM: Remote and local processes. *Int J Climatol* (In press).
- 592 Cherchi A, Masina S and Navarra A (2008) Impact of extreme CO<sub>2</sub> levels on tropical climate: A CGCM  
593 study. *Clim Dyn* 31: 743–758
- 594 Deser C, Phillips AS, Tomas RA, Okumura YM, Alexander MA, Capotondi A, Scott JD, Kwon Y, Ohba  
595 M (2012) ENSO and Pacific Decadal Variability in the Community Climate System Model Version 4. *J*  
596 *Clim* 25(8): 2622–2651
- 597 Deser C, Alexander MA, Xie SP, Phillips AS (2010) Sea Surface Temperature Variability: Patterns and

598 Mechanisms. *Ann Rev Marine Sc* 2: 115–143

599 Fogt R, Bromwich D (2006) Decadal variability of the ENSO teleconnection to the high-latitude South  
600 Pacific governed by coupling with the Southern Annular Mode. *J Clim* 19: 979–997

601 Grimm A (2003) The El Nino impact on the summer monsoon in Brazil: Regional processes versus remote  
602 influences. *J Climate*, 16, 263-280

603 Grimm A, Barros VR, Doyle ME (2000) Climate variability in southern South America associated with El  
604 Nino and La Nina events. *J Climate*, 13, 35-58

605 Gualdi S, E Scoccimarro and A Navarra (2008) Changes in Tropical Cyclone Activity due to Global Warm-  
606 ing: Results from a High-Resolution Coupled General Circulation Model. *J Climate* 21 5204-5228

607 Huang HP, Seager R, Kushnir Y (2005) The 1976/77 transition in precipitation over the Americas and the  
608 influence of tropical sea surface temperature. *Clim Dyn*, 24, 721-740

609 Kalnay E, Kanamitsu M, Kistler R, and co-authors (1996) The NCEP/NCAR 40-Year Reanalysis Project.  
610 *Bull Am Meteor Soc* 77 437-471

611 Liebmann B, and co-authors (2004) An observed trend in central South American precipitation. *J Clim* 17:  
612 4357–4367

613 Madec, G., P. Delecluse, M. Imbard and C. Levy, 1998: OPA version 8.1 Ocean General Circulation Model  
614 reference manual. *Technical report*, LODYC/IPSL Note 11.

615 Marshall GJ (2003) Trends in the Southern Annular Mode from Observations and Reanalyses. *J Clim* 16:  
616 4134–4143

617 Menéndez G, Carril AF (2010) Potential changes in extremes and links with the Southern Annular Mode as  
618 simulated by a multi-model ensemble. *Clim Change* 98(3): 359–377 DOI 10.1007/s10584-009-9735-7

619 Mitchell TD, Jones PD (2005) An improved method of constructing a database of monthly climate obser-  
620 vations and associated high-resolution grids. *Int J Climatol* 25 693–712

621 Mo KC (2000)

622 Mo KC, Paegle JN (2001) The Pacific-South American modes and their downstream effects. *Int J Climatol*  
623 21: 1211–1229

624 Navarra A, Gualdi S, Masina S, Behera S, Luo J-J, Masson S, Guilyardi E, Delecluse P, Yamagata T (2008)  
625 Atmospheric horizontal resolution affects tropical climate variability in coupled models. *J Clim* 21: 730–  
626 750

627 Paegle JN, Mo KC (2002) Linkages between summer rainfall variability over South America and sea surface  
628 temperature anomalies. *J Climate*, 15, 1389-1407

629 Rayner NA, Parker DE, Horton EB, Folland CK, Alexander LV, Rowell DP, Kent EC, Kaplan A (2003)

630 Global analysis of sea surface temperature, sea ice and night marine air temperature since the late nine-  
631 teenth century. *J Geophys Res* 18(D14): 4407 DOI:10.1029/2002JD002670

632 Robertson AW, Mechoso CR (2000) Interannual and interdecadal variability of the South Atlantic conver-  
633 gence zone. *Mon Wea Rev* 128: 2947–2957

634 Roeckner, E., K. Arpe, L. Bengtsson, M. Christoph, M. Claussen, L. Dümenil, M. Esch, M. Giorgetta,  
635 U. Schlese and U. Schulzweida, 1996: The Atmospheric general circulation Model ECHAM4: Model  
636 description and simulation of present-day climate: *Max-Planck Institut für Meteorologie*, Report no. 218,  
637 Hamburg, 86 pp.

638 Rusticucci M, Penalba O (2000) Interdecadal changes in the precipitation seasonal cycle over southern  
639 South America and their relationship with surface temperature. *Climate Res* 16: 1–15

640 Seager R, Naik N, Baethgen W, Robertson A, Kushnir Y, Nakamura J, Jurburg S (2010) Tropical oceanic  
641 causes of interannual to multidecadal precipitation variability in Southeast South America over the past  
642 century. *J Climate*, 23, 5517-5539

643 Silva GAM, Ambrizzi T, Marengo JA (2009) Observational evidences on the modulation of the South  
644 American Low Level Jet east of the Andes according the ENSO variability. *Ann Geophys* 27: 645–657

645 Silvestri GE (2004) El Nino signal variability in the precipitation over Southeastern South America during  
646 austral summer. *Geophys Res Lett* 31 doi:10.1029/2004GL020590

647 Silvestri G, Vera C (2009) Non-stationarity impacts of the Southern Annular Mode on Southern Hemisphere  
648 climate. *J Climate*, 22, 6142-6148

649 Silvestri G, Vera C (2008) Evaluation of the WCRP-CMIP3 model simulations in the La Plata basin. *Met*  
650 *Appl*, 15, 497-502

651 Silvestri G, Vera C (2003) Antarctic oscillation signal on precipitation anomalies over southeastern South  
652 America. *Geophys Res Lett* 30: 2115 doi:10.1029/2003GL018277

653 Stuck J, A Guntner, B Merz (2006) ENSO impact on simulated South American hydro-climatology. *Adv in*  
654 *Geosciences* 6: 227–336

655 Taschetto AS, Ambrizzi T (2012) Can Indian Ocean SST anomalies influence South American rainfall?  
656 *Clim Dyn* 38: 1615–1628 DOI:10.1007/s00832-0111-1165-3

657 Thompson D, Wallace J (2000) Annular modes in the extratropical circulation. Part I: Month-to-month  
658 variability. *J Clim* 13: 1000–1016

659 Vera C, Silvestri G (2009) Precipitation interannual variability in South America from the WCRP-CMIP3  
660 multi-model dataset. *Clim Dyn*, 32, 1003-1014

661 Vera C, Silvestri G, Liebmann B, Gonzalez P (2006) Climate change scenarios for seasonal pre-

662     precipitation in South America from the IPCC AR4 models. *Geophys Res Lett*, 33, L13707,  
663     DOI:10.1029/2006GL025759

664 Vera C, Silvestri G, Barros V, Carril AF (2004) Differences in El Nino response over the Southern Hemi-  
665     sphere. *J Climate*, 17, 1741–1753

666 Xie P, Arkin PA (1997) Global precipitation: A 17-year monthly analysis based on gauge observations,  
667     satellite estimates, and numerical model outputs. *Bull Amer Meteor Soc* 78: 2539–2558

668 Yulaeva E, Wallace JM (1994) The signature of ENSO in global temperature and precipitation fields derived  
669     from the Microwave Sounding Unit. *J Clim* 7: 1719–1736

670 Zamboni L, Cherchi A, Barreiro M, Kucharski F (2012) Dynamics of the impact of ENSO flavors on  
671     precipitation over La Plata Basin. Under review on *Climate Dynamics*

672 Zamboni L, Kucharski F, Mechoso CR (2011) Seasonal variations of the links between the interannual  
673     variability of South America and the South Pacific. *Clim Dyn* 38(9): 2115–2129 DOI 10.1007/s00382-  
674     011-1116-zn

675 Zamboni L, Mechoso CR, Kucharski F (2010) Relationships between upper-level circulation over South  
676     America and rainfall over Southeastern South America: A physical base for seasonal predictions. *J Clim*  
677     23: 3300–3315

678 Zhou J, Lau KM (2001) Principal modes of interannual and decadal variability of summer rainfall over  
679     South America. *Int J Climatol* 21: 1623–1644

680 Zhou J, Lau KM (2002) Intercomparison of model simulations of the impact of 1997/98 El Nino on South  
681     American summer monsoon. *Meteorologica* 27: 99–116

precip (mm/d)	SA OND mean	SA OND std	LPB OND mean	LPB OND std
CRU	4.52	0.44	4.12	1.02
AMIP-type	4.35	0.31	4.68	0.80
SSXX	4.26	0.77	4.44	0.88

**Table 1.** OND mean precipitation and its standard deviation (mm/d) averaged over the South American continent (SA) and over the La Plata Basin (LPB) region (65-47W, 37-19S) for CRU dataset (first row), AMIP-type ensemble (second row) and SSXX experiment (third row).

	PC1(CRU)	PC2(CRU)	PC3(CRU)
PC1(CMAP)	-0.94*	-0.23	0.00
PC2(CMAP)	-0.17	0.67*	0.42
PC3(CMAP)	-0.11	0.33	-0.80*

**Table 2.** Correlation coefficients of South America OND precipitation anomalies first three principal components (PC1, PC2 and PC3) for the period 1979-2005 between CRU and CMAP datasets. An asterisk marks the values that are statistical significant at 95%.

	PC1	PC2	PC3
EXP01	0.60	-0.50	-0.36
EXP02	0.32	-0.57	-0.38
EXP03	0.40	-0.63	-0.09
EXP04	0.63	-0.38	-0.13
EXP05	0.44	-0.55	-0.06
EXP06	0.44	-0.42	-0.23
EXP07	0.52	-0.53	0.07
EXP08	0.54	-0.48	-0.29
EXP09	0.66	-0.41	-0.19
Mean of corr	0.55	-0.50	-0.18

**Table 3.** Correlation coefficients between NINO3.4 index and OND SA precipitation principal components for the AMIP-type ensemble. Values are reported for each member of the ensemble, including the mean in the bottom.

	$\omega$ 500 (mb/s)	u200 (m/s)
In Phase Pos	0.65	2.82
Out Phase Pos	0.09	1.35
Partial Phase Pos	0.19	2.27
In Phase Neg	-0.26	-0.84
Out Phase Neg	-0.08	-0.17
Partial Phase Neg	-0.21	-0.75

**Table 4.** Averages of vertical velocity ( $\omega$ , mb/s) at 500 mb in the region Eq-20S, 75W-55W (2nd column) and of zonal velocity (m/s) at 200 mb in the region 20S-40S, 90W-60W (3rd column) for the In Phase Positive, Out of Phase Positive, Partial in Phase Positive, In Phase Negative, Out of Phase Negative and Partial in Phase Negative (from top to bottom) composites.

	Wet LPB yrs	Dry LPB yrs
In Phase	1951(4) 1963(1) 1982(9) 1997(4) 2002(5)	1971(1) 1985(2) 1989(2) 1999(4)
Out of Phase	1961(3) 1963(2) 1997(1) 2002(2) 2003(8)	1948(6) 1955(3) 1956(4) 1962(4) 1971(3) 1985(2)

**Table 5.** List of years where the model PC1 is "In Phase" (exceeding 1 standard deviation in the same direction) or "Out of Phase" (exceeding 1 standard deviation in the opposite direction) with the CRU PC1. Years are separated for wet LPB years (i.e. positive PC1 values) and for dry LPB years (i.e. negative PC1 values). Within each year the number of members having the same behavior is indicated in parentheses.

**Fig. 1.** First three EOFs of OND mean South American precipitation (in the box shown but considering land-points only) for the period 1979-2005 for CRU (upper panels) and XieArkin (lower panels) dataset, respectively.

**Fig. 2.** First three EOFs modes and principal components (PCs) of OND South American precipitation (in the box shown but considering land-points only) for CRU dataset from 1948 to 2003.

**Fig. 3.** EOFs (1st and 2nd modes) of OND South American precipitation (in the box shown considering land-points only) for AMIP-type ensemble.

**Fig. 4.** Time-correlation coefficients of OND South America precipitation PC1 and OND SST for (a) HadISST/CRU datasets, (b) AMIP-type ensemble and (c) coupled model experiment (SSXX).

**Fig. 5.** Same as fig. 4 but a 7-years low-pass filter is applied to the PC1.

**Fig. 6.** 19 years sliding correlation (x-axis shows the first year of the 19 years interval) between SAM and LPB precipitation during OND for observations based on SLP (magenta line) and for the AMIP-type ensemble (black lines). Solid and dashed black lines represent the correlation applied to the ensemble mean and to the average of the correlation applied to each member of the ensemble, respectively. The horizontal solid lines correspond to the threshold values statistically significant at 95%.

**Fig. 7.** Composite anomalies of SST ( $^{\circ}\text{C}$ , shaded) and 200 mb eddy streamfunction ( $10^6 \text{ m}^2/\text{s}$ , contours) composite anomalies for wet and dry LPB years in (a,b) HadISST/CRU datasets and (c,d) AMIP-type ensemble.

**Fig. 8.** Composite anomalies of SST ( $^{\circ}\text{C}$ , shaded) and 200 mb eddy streamfunction ( $10^6 \text{ m}^2/\text{s}$ , contours) for wet (positive) and dry (negative) LPB years in AMIP-type ensemble members grouped as (a,b) "In Phase", (c,d) "Out of Phase" and (e,f) "Partial In Phase" PC1 values (the classification is described in the text).

**Fig. 9.** Same as fig. 8 but for vertically integrated moisture ( $\text{kg/m}^2$ , shaded) and vertically integrated moisture flux ( $\text{kg/m s}$ , vectors).

**Fig. 10.** 1982 OND composite of (a) SST ( $^{\circ}\text{C}$ , shaded) and 200 mb eddy streamfunction ( $10^6 \text{ m}^2/\text{s}$ , contours), (b) precipitation ( $\text{mm/d}$ , shaded) and 850 mb wind ( $\text{m/s}$ , vectors) and (c) 1982 OND standard deviation among members of 200 mb streamfunction ( $10^6 \text{ m}^2/\text{s}$ ) for the AMIP-type ensemble.

**Fig. 11.** OND 2003 SST ( $^{\circ}\text{C}$ , shaded) and 200 mb eddy streamfunction ( $10^6 \text{ m}^2/\text{s}$ , contours) (left) and precipitation ( $\text{mm/d}$ , shaded) and 850 mb wind ( $\text{m/s}$ , vectors) (right) for (a,b) HadISST/CRU/NCEP datasets and (c,d) AMIP-type ensemble composite. (e) OND 2003 standard deviation among members of 200 mb streamfunction ( $10^6 \text{ m}^2/\text{s}$ ) in the AMIP-type ensemble.

**Fig. 12.** OND 2003 200 mb eddy streamfunction ( $10^6 \text{ m}^2/\text{s}$ ) for (a-i) each member of the AMIP-type ensemble (from #1 to #9) and (l) for the ensemble mean (bottom right panel).

**Fig. 13.** OND 1999 SST ( $^{\circ}\text{C}$ , shaded) and 200 mb eddy streamfunction ( $10^6 \text{ m}^2/\text{s}$ , contours) (left) and precipitation ( $\text{mm/d}$ , shaded) and 850 mb wind ( $\text{m/s}$ , vectors) (right) for (a,b) HadISST/CRU/NCEP datasets and (c,d) AMIP-type ensemble composite. (e) OND 1999 standard deviation among members of 200 mb streamfunction ( $10^6 \text{ m}^2/\text{s}$ ) in the AMIP-type ensemble.

**Fig. 14.** OND 1999 precipitation ( $\text{mm/d}$ , shaded) and 200 mb eddy streamfunction ( $10^6 \text{ m}^2/\text{s}$ , contours) for (a-i) each member of the AMIP-type ensemble (from #1 to #9) and (l) fro the ensemble mean (bottom right panel).

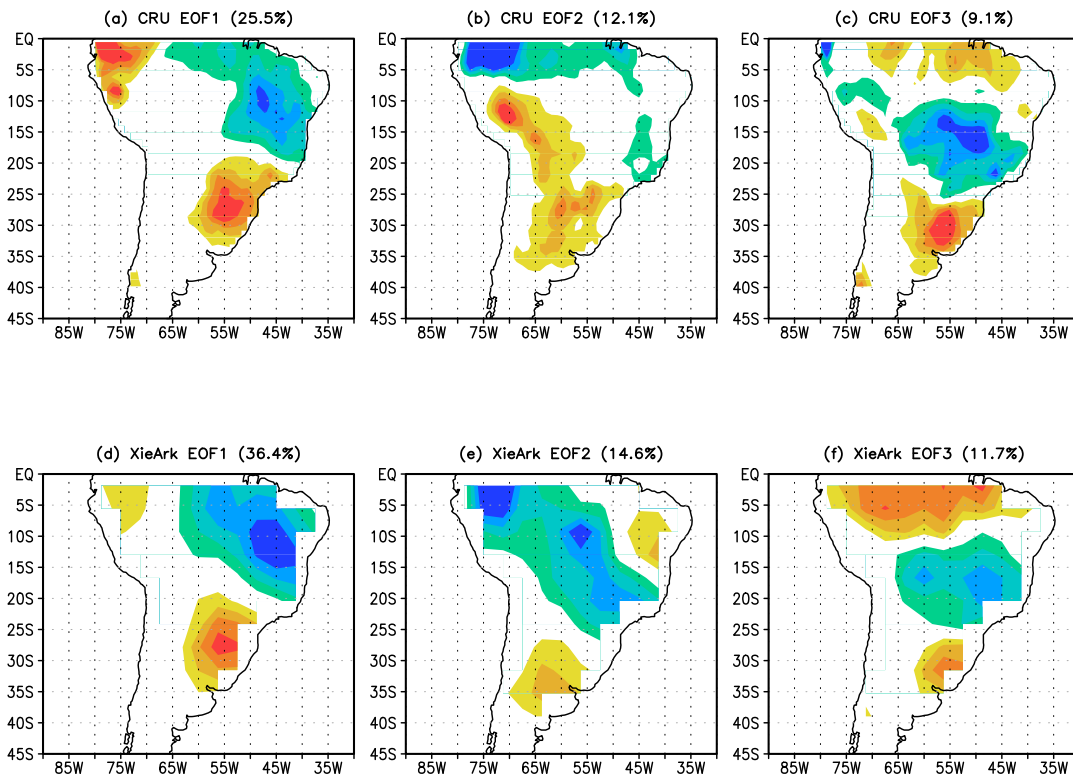


**Fig. 1.** First three EOFs of OND mean South American precipitation (in the box shown but considering land-points only) for the period 1979-2005 for CRU (upper panels) and XieArkin (lower panels) dataset, respectively.

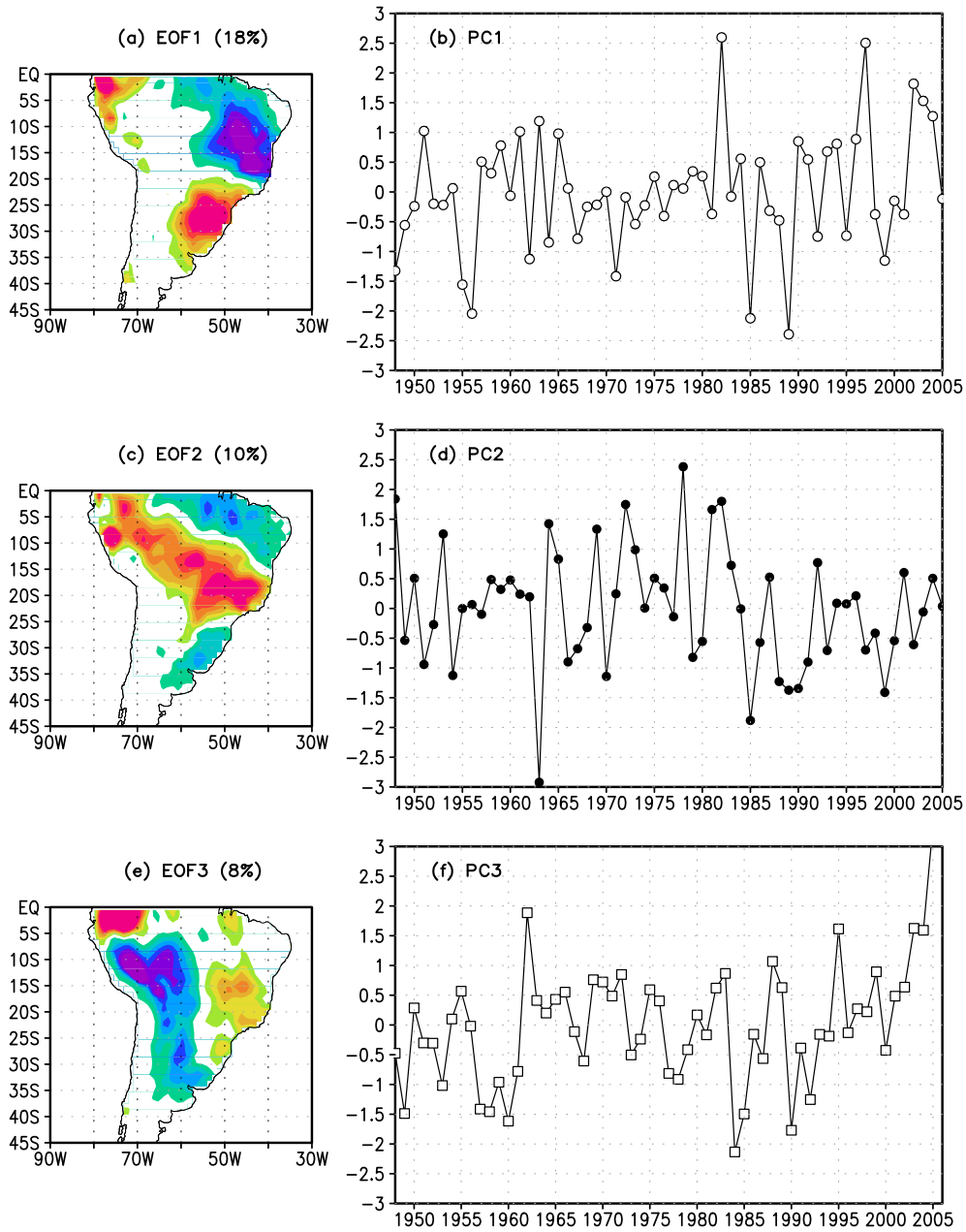


**Fig. 2.** First three EOFs modes and principal components (PCs) of OND South American precipitation (in the box shown but considering land-points only) for CRU dataset from 1948 to 2003.

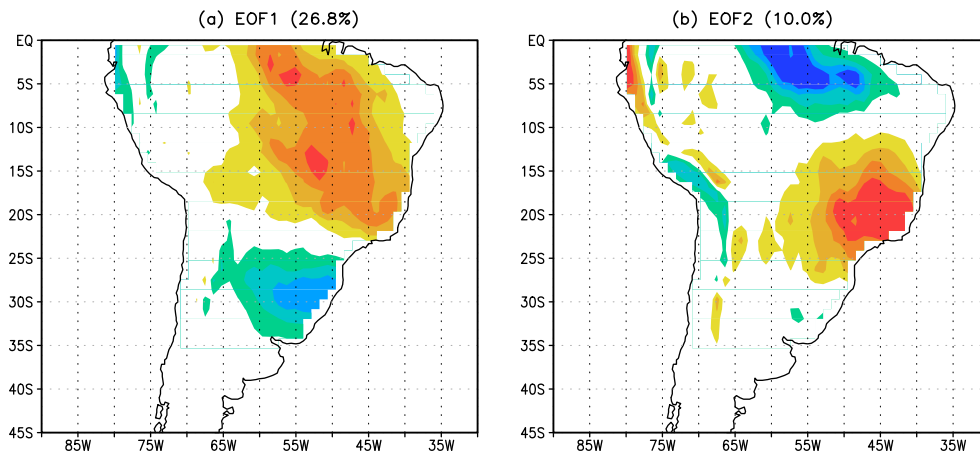


**Fig. 3.** EOFs (1st and 2nd modes) of OND South American precipitation (in the box shown considering land-points only) for AMIP-type ensemble.

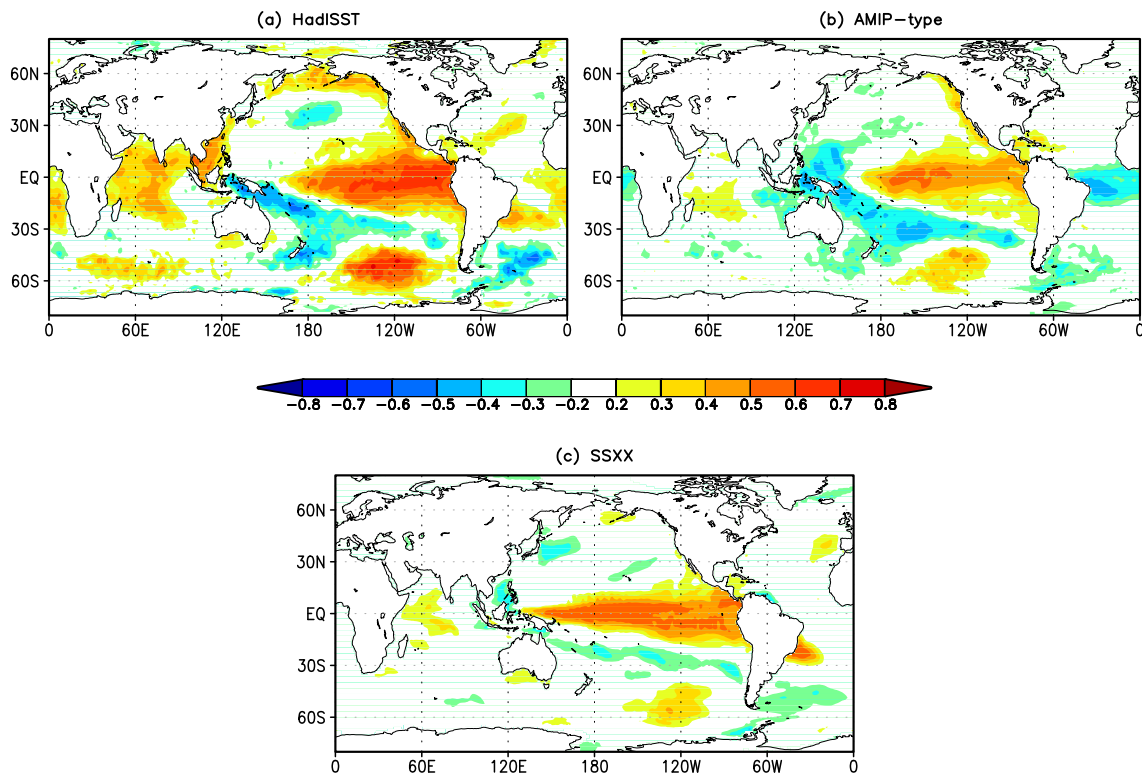


**Fig. 4.** Time-correlation coefficients of OND South America precipitation PC1 and OND SST for (a) HadISST/CRU datasets, (b) AMIP-type ensemble and (c) coupled model experiment (SSXX).

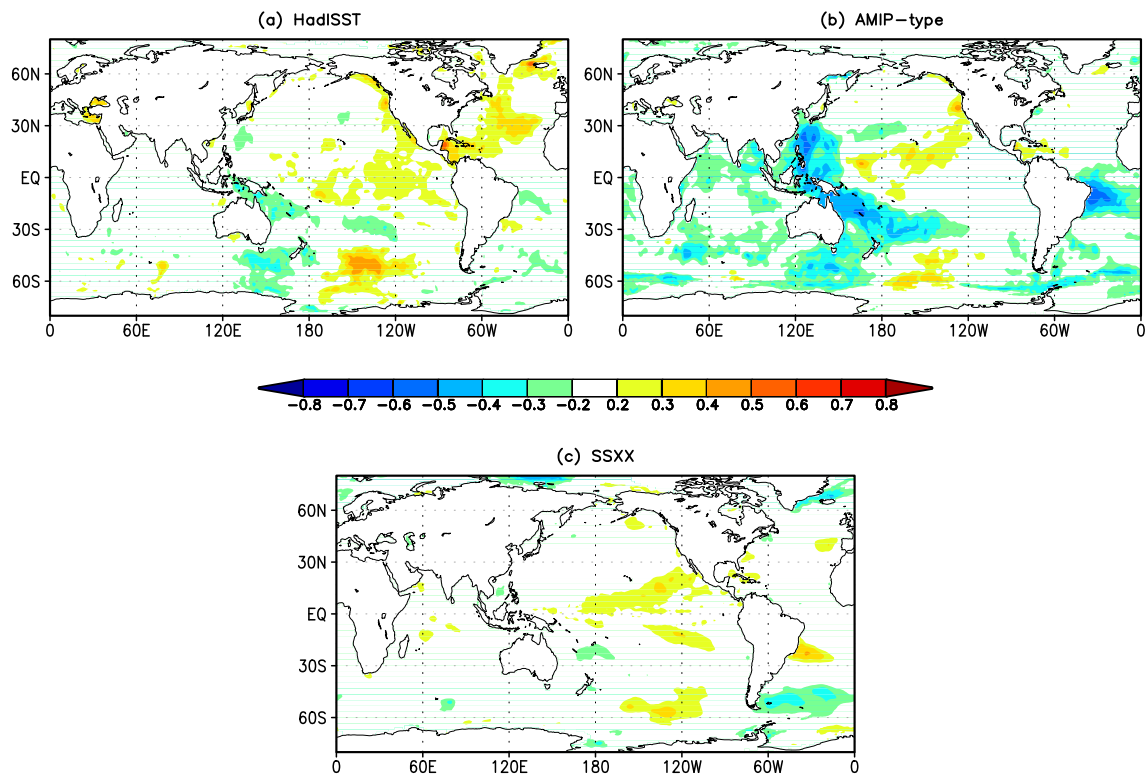


**Fig. 5.** Same as fig. 4 but a 7-years low-pass filter is applied to the PC1.

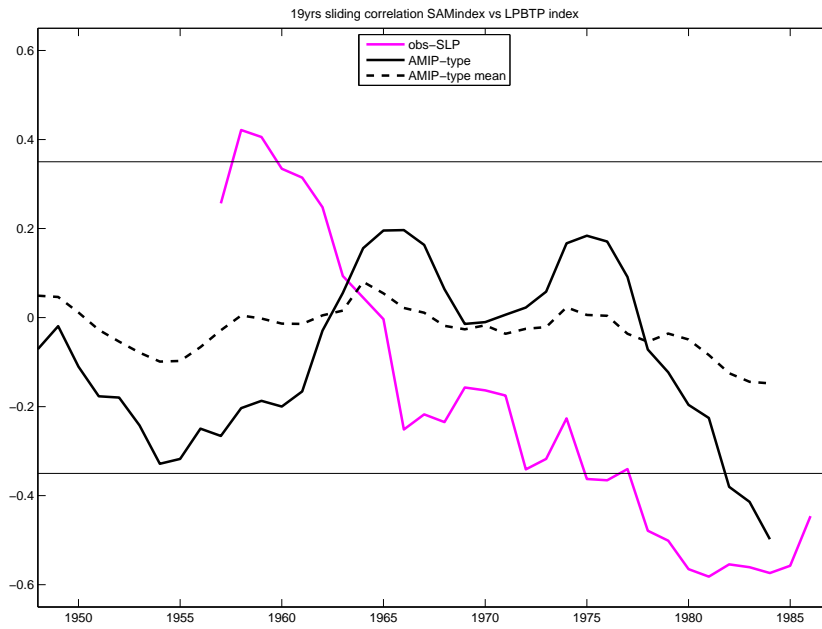


**Fig. 6.** 19 years sliding correlation (x-axis shows the first year of the 19 years interval) between SAM and LPB precipitation during OND for observations based on SLP (magenta line) and for the AMIP-type ensemble (black lines). Solid and dashed black lines represent the correlation applied to the ensemble mean and to the average of the correlation applied to each member of the ensemble, respectively. The horizontal solid lines correspond to the threshold values statistically significant at 95%.

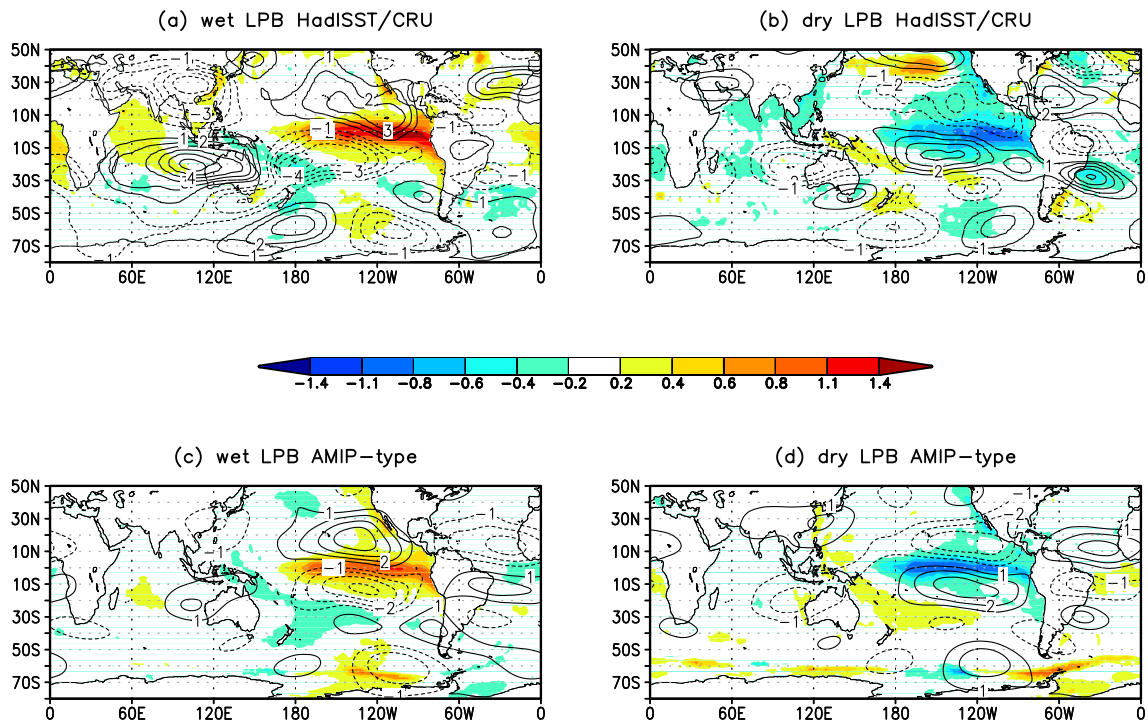


**Fig. 7.** Composite anomalies of SST ( $^{\circ}\text{C}$ , shaded) and 200 mb eddy streamfunction ( $10^6 \text{ m}^2/\text{s}$ , contours) composite anomalies for wet and dry LPB years in (a,b) HadISST/CRU datasets and (c,d) AMIP-type ensemble.

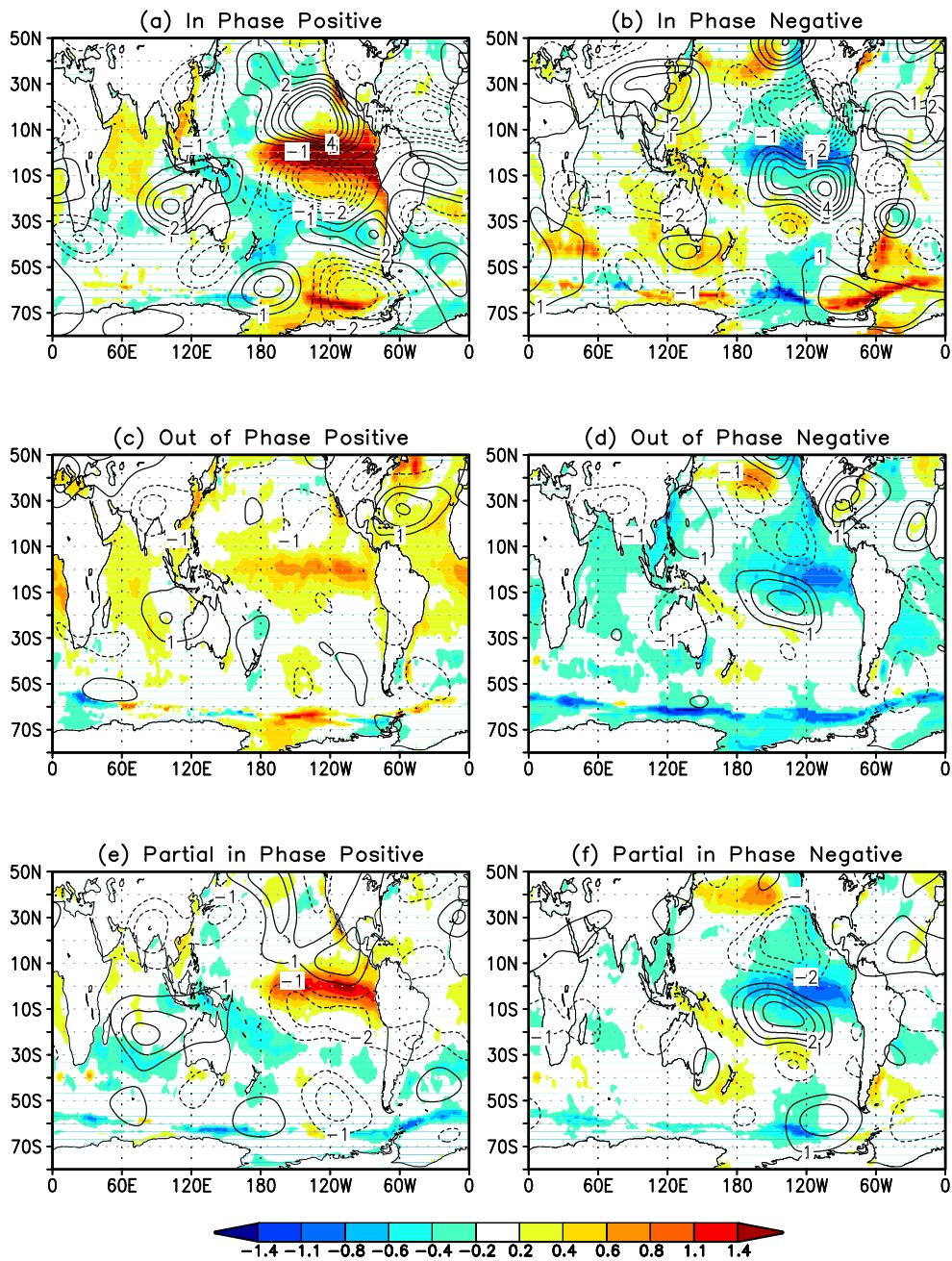


**Fig. 8.** Composite anomalies of SST ( $^{\circ}\text{C}$ , shaded) and 200 mb eddy streamfunction ( $10^6 \text{ m}^2/\text{s}$ , contours) for wet (positive) and dry (negative) LPB years in AMIP-type ensemble members grouped as (a,b) "In Phase", (c,d) "Out of Phase" and (e,f) "Partial In Phase" PC1 values (the classification is described in the text).

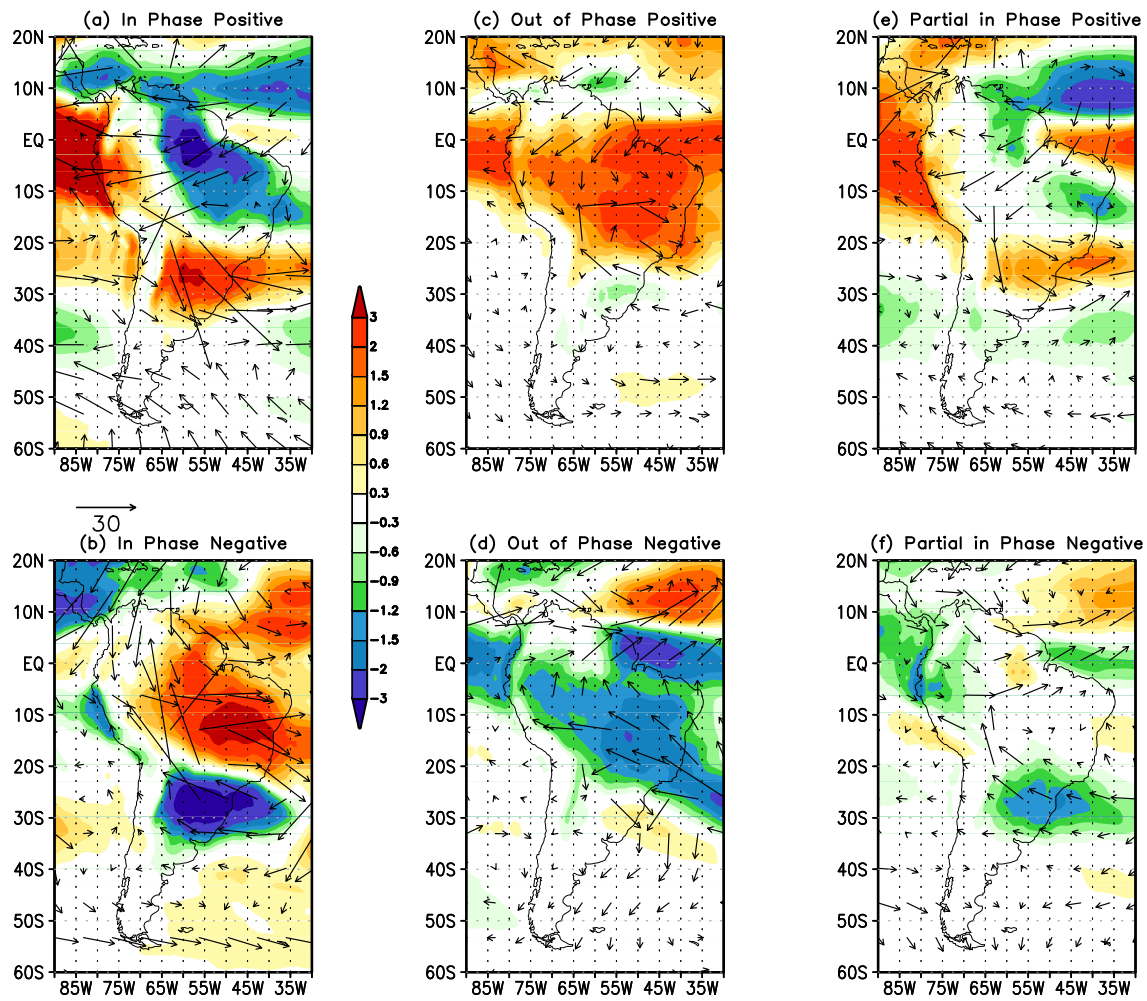


**Fig. 9.** Same as fig. 8 but for vertically integrated moisture ( $\text{kg/m}^2$ , shaded) and vertically integrated moisture flux ( $\text{kg/m s}$ , vectors).

CASE STUDY 1982 – AMIP-type

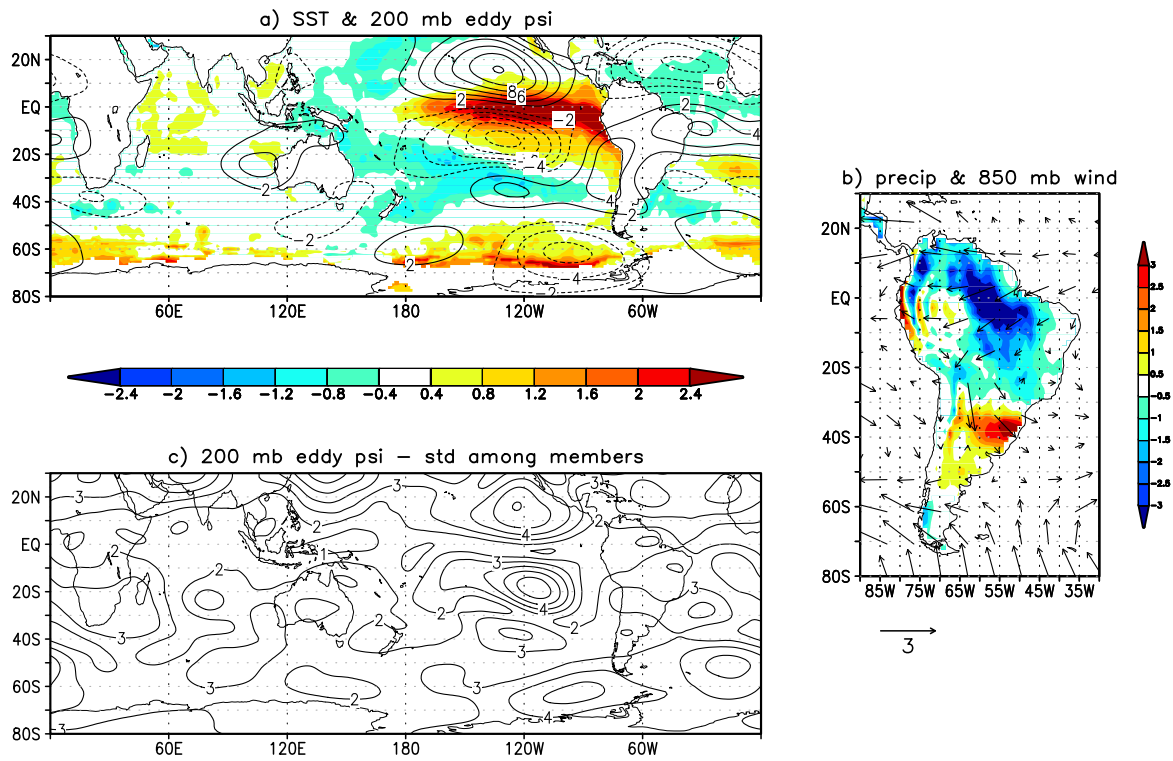


**Fig. 10.** 1982 OND composite of (a) SST ( $^{\circ}\text{C}$ , shaded) and 200 mb eddy streamfunction ( $10^6 \text{ m}^2/\text{s}$ , contours), (b) precipitation (mm/d, shaded) and 850 mb wind (m/s, vectors) and (c) 1982 OND standard deviation among members of 200 mb streamfunction ( $10^6 \text{ m}^2/\text{s}$ ) for the AMIP-type ensemble.

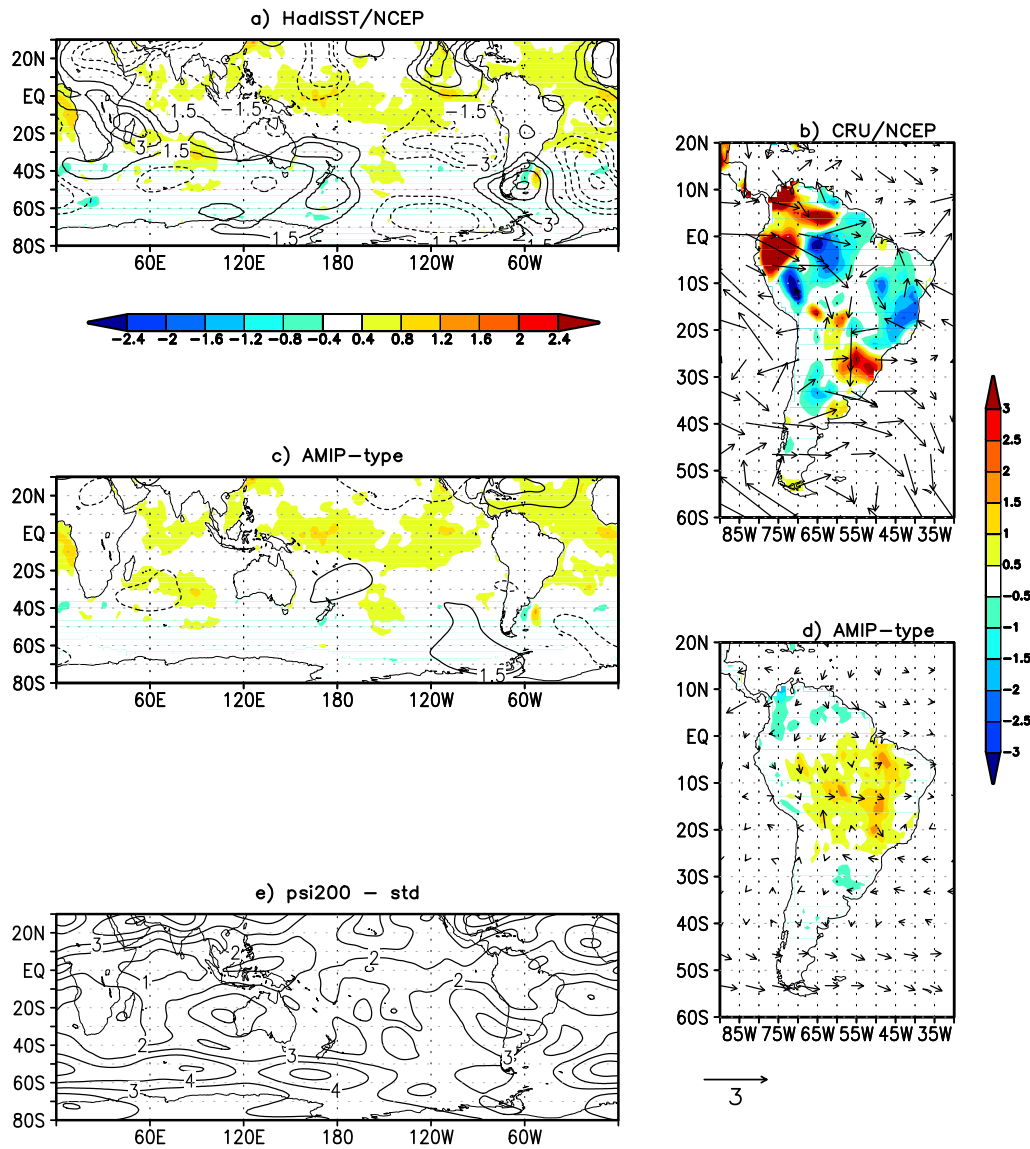


**Fig. 11.** OND 2003 SST ( $^{\circ}\text{C}$ , shaded) and 200 mb eddy streamfunction ( $10^6 \text{ m}^2/\text{s}$ , contours) (left) and precipitation (mm/d, shaded) and 850 mb wind (m/s, vectors) (right) for (a,b) HadISST/CRU/NCEP datasets and (c,d) AMIP-type ensemble composite. (e) OND 2003 standard deviation among members of 200 mb streamfunction ( $10^6 \text{ m}^2/\text{s}$ ) in the AMIP-type ensemble.

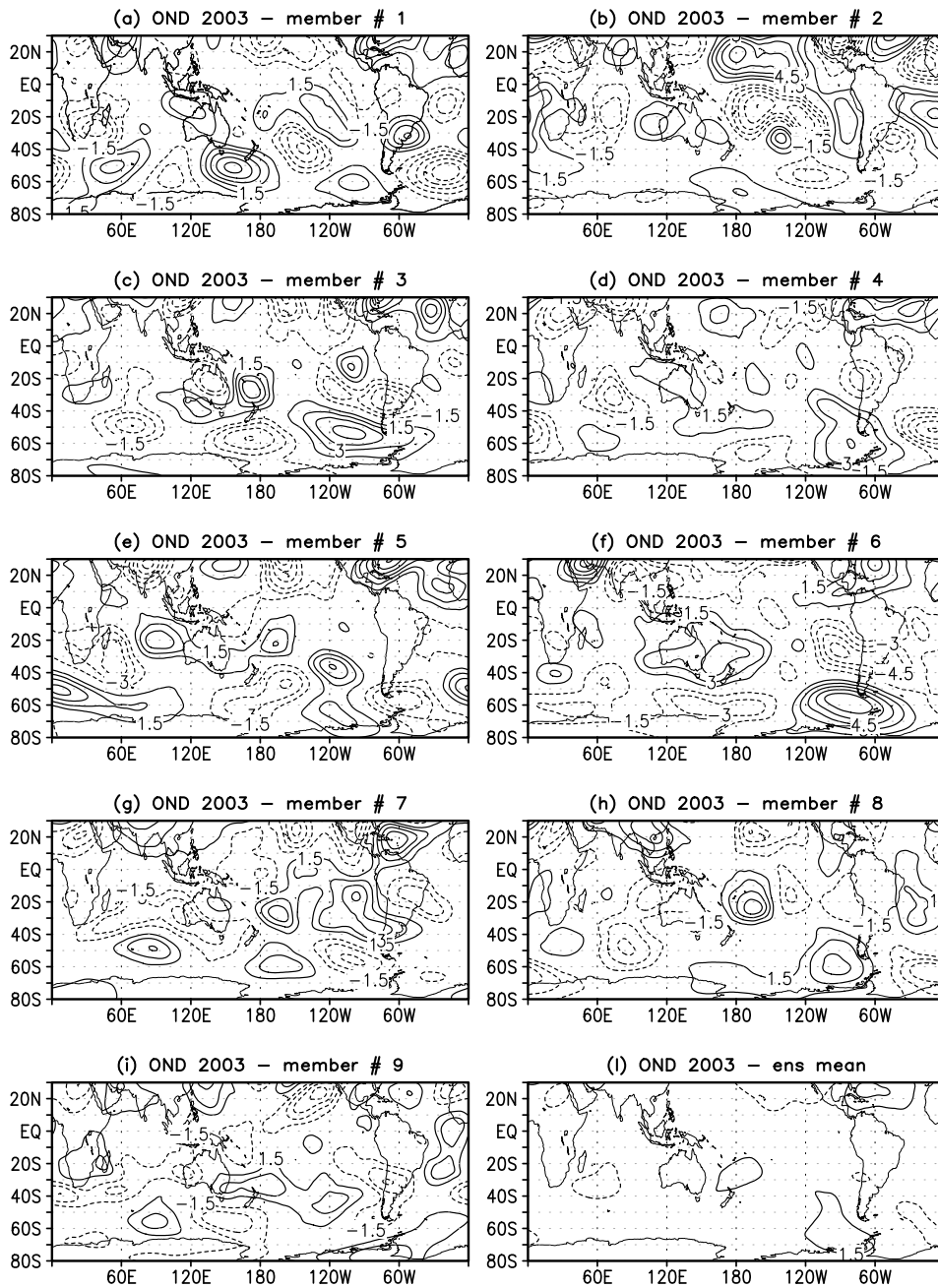


**Fig. 12.** OND 2003 200 mb eddy streamfunction ( $10^6 \text{ m}^2/\text{s}$ ) for (a-i) each member of the AMIP-type ensemble (from #1 to #9) and (i) for the ensemble mean (bottom right panel).

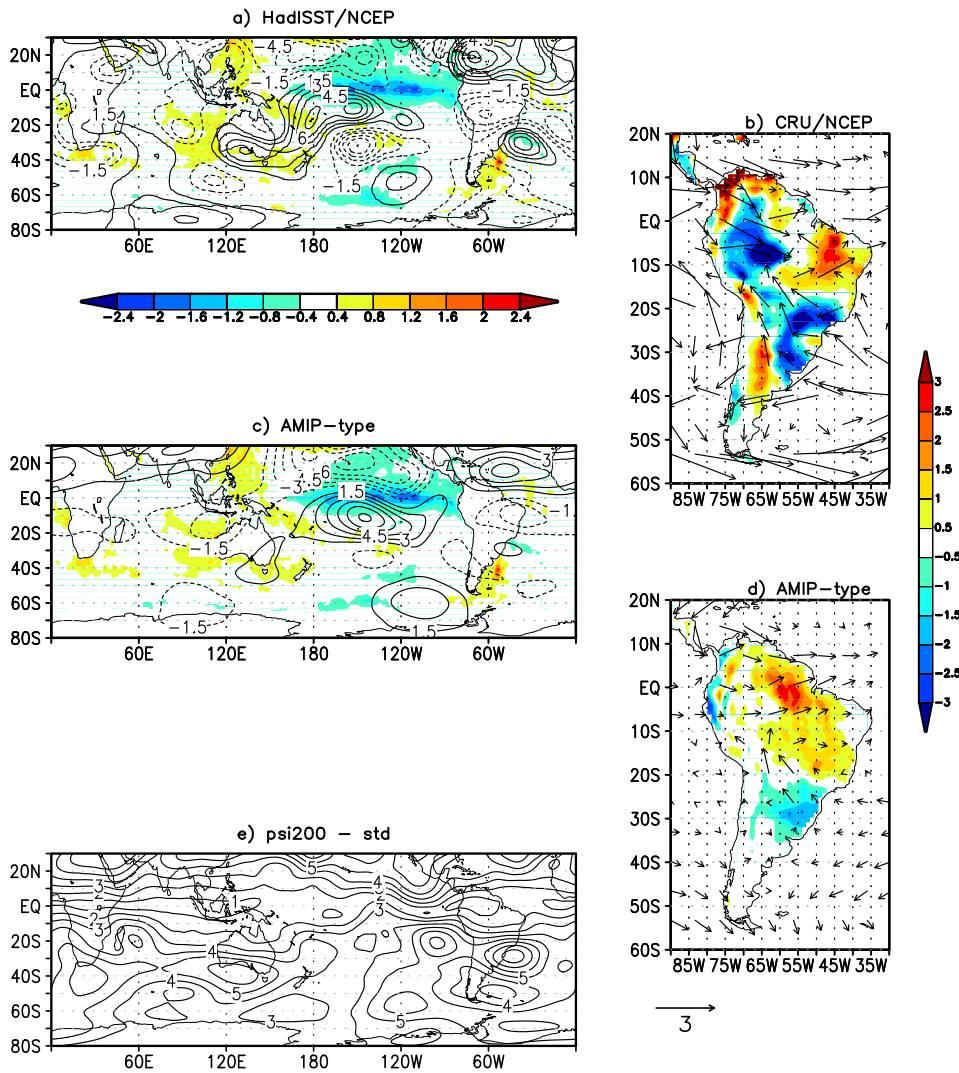


**Fig. 13.** OND 1999 SST ( $^{\circ}\text{C}$ , shaded) and 200 mb eddy streamfunction ( $10^6 \text{ m}^2/\text{s}$ , contours) (left) and precipitation (mm/d, shaded) and 850 mb wind (m/s, vectors) (right) for (a,b) HadISST/CRU/NCEP datasets and (c,d) AMIP-type ensemble composite. (e) OND 1999 standard deviation among members of 200 mb streamfunction ( $10^6 \text{ m}^2/\text{s}$ ) in the AMIP-type ensemble.

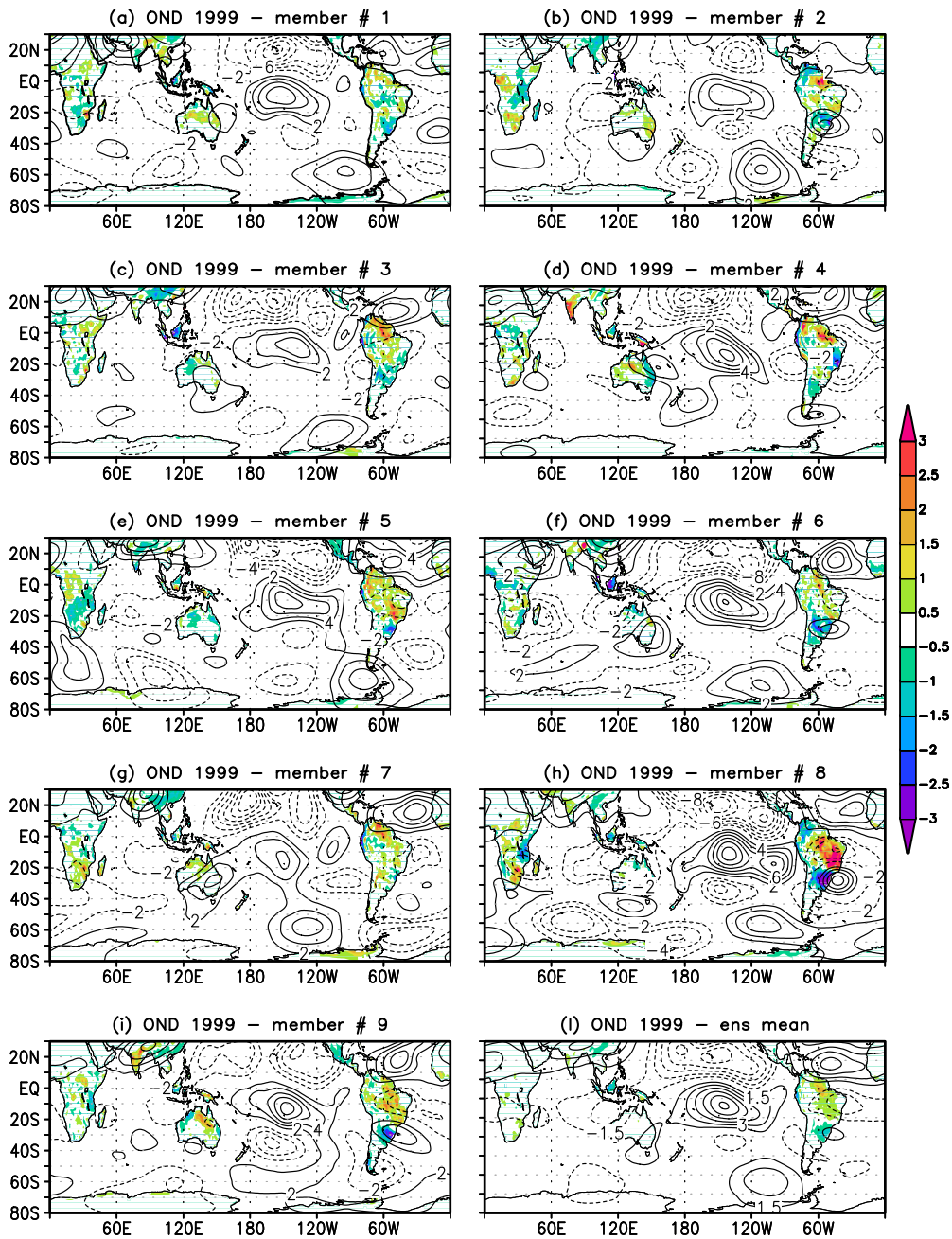


**Fig. 14.** OND 1999 precipitation (mm/d, shaded) and 200 mb eddy streamfunction ( $10^6 \text{ m}^2/\text{s}$ , contours) for (a-i) each member of the AMIP-type ensemble (from #1 to #9) and (l) from the ensemble mean (bottom right panel).